Development and Implementation of Laboratory Test Methods for the Evaluation of Wearable Head Impact Sensors

Abigail M. Tyson

Thesis submitted to the faculty of the Virginia Polytechnic Institute and State University in partial fulfillment of the requirements for the degree of

Master of Science
In
Biomedical Engineering and Mechanics

Stefan M. Duma, Committee Chair
Steven Rowson, Co-Chair
Andrew R. Kemper

December 7, 2015
Blacksburg, VA

Keywords: concussion, head impacts, sensor, youth sports, unhelmeted sports

Development and Implementation of Laboratory Test Methods for the Evaluation of Wearable Head Impact Sensors

Abigail M. Tyson

ABSTRACT

With a rise in wearable sensor technology and the desire to investigate head impacts in previously unstudied groups, wearable head impact sensors have reached nation-wide popularity for their promising benefits to consumers and researchers. However, there are risks in relying on such technology before proper validation of its performance has been completed. Preliminary tests have found that current sensors vary widely in performance. The objective of this work was to develop and implement a test method for evaluation of wearable sensors in an ideal laboratory environment. A custom pendulum was used to impact a NOCSAE headform mounted on a Hybrid III neck. Sensors were tested under helmeted and unhelmeted conditions, according to their prescribed use. The headform was impacted at four locations, each at four impact energies ranging from 25 g to 100 g. Peak and time series headform kinematics output by each sensor were compared to accelerometers and angular rate sensors inside the headform. Average and standard deviations of peak sensor error and normalized RMS error were evaluated at each test condition to describe sensor performance. Requirements were set in the slope and coefficient of determination from linear regressions constrained through the origin to describe adequate sensor performance under ideal conditions. Sensors that met the requirement in at least one kinematic variable will be further evaluated in more realistic on-field and cadaver tests. The combination of all testing phases will be used to provide an overall sensor evaluation for both researchers and consumers.

DEDICATION

With gratitude for God, my husband, family, and friends; all those who have kept me centered and focused on the truly important things in life.

~

A special thanks to Dr. Stefan Duma, Dr. Steve Rowson, and Dr. Andrew Kemper for their guidance and for the opportunities to learn and be challenged.

I also thank all my fellow graduate students, especially Bryan Cobb, Stephanie Beeman, and Vanessa Alphonse, for their daily help in my never-ending questions. I am also grateful for the assistance of Bryan, Bethany Rowson, Jaclyn Press, and Megan Bland during long days of testing.

Lastly, heartfelt thanks to Tina Garman for her statistical advice and her patience, help, and encouragement in finishing this thesis.

TABLE OF CONTENTS

LIST OF FIGURES

LIST OF TABLES

INTRODUCTION

CONCUSSION EPIDEMIOLOGY AND RISK

As many as 3.8 million sports-related concussions are estimated to occur each year in the United States.[1] While acute symptoms may persist for days to weeks following a concussion, recent research has suggested repetitive concussive and subconcussive impacts may result in long-term neurodegeneration.[2-4] Despite measures to increase public knowledge of concussions in recent years[5], there is still over 50% symptom under-reporting among athletes.[6-9] These athletes prolong their recovery and put themselves at higher risk of long-term damage.[10,11] Medical professionals on the sideline benefit athletes by being available to diagnose concussions soon after they occur[12], yet this is still only a privilege for professional, collegiate, and affluent high school teams.[13] Of all athletes in the United States per year, over 45 million are between the age of 6 and 18[14] but only 460,000 play at the varsity collegiate level.[15] Although youth athletes make up the largest population in sports by far, they are also the demographic with the least accessibility to immediate medical attention.[16,17]

WEARABLE HEAD IMPACT SENSORS

To provide an objective measure of head impact magnitude, companies have developed wearable head impact sensors for on-field play. Although these sensors cannot themselves diagnose a concussion, they can provide additional information to a coach or medical professional as to the severity of an impact. Researchers also have interest in wearable head impact sensors to shed further light on the biomechanics of concussions. One such widely-used sensor is the Head Impact Telemetry (HIT) System. Duma et al.[18] first instrumented collegiate football athletes with this System in 2003, and have since collected over 1.5 million head impacts together with other high schools and universities.[18] As the result of various studies using the HIT System, risk curves for concussion have been developed for adult male athletes[19-22] and rule changes have been implemented in Pop Warner[23,24] and the NFL[25,26] to decrease high impact events. The drawbacks to this System are that it is expensive to implement for an entire team and it is only widely used in football. Within collegiate sports, similar concussion rates occur in football, ice hockey, lacrosse, and soccer for both men and women[27,28], although only football has received top media attention and research efforts.

As a result of the increased awareness of sports concussions in recent years and the advancements in technology that make wearable sensors more accessible to consumers, there has been a flood of new, inexpensive, user-friendly wearable head impact sensors for a variety of sports applications. In addition to consumer interest, researchers have also been in pursuit of a reliable sensor for unhelmeted sports. Higher concussion rates among women in some sports have led researchers to believe different factors play a role in concussions in women compared to men. These may include a woman's smaller mass, lower neck strength, or hormonal influences.[29,30]

Currently available wearable head impact sensors vary in their applications and capabilities. Some simply alert a player or coach of a severe impact via light or vibration while others output full head kinematics for each impact. The placement of each sensor also varies. The most common include those mounted on a helmet shell, in a headband or skull cap, adhered to the skin as a patch, or worn as a mouth guard.[31-35]

RESEARCH OBJECTIVES

With a surge in wearable impact sensors coupled with increasing knowledge of the potential risks of sport-related concussions, most athletes will likely be wearing sensors within the next five to ten years. Unfortunately, the accuracy and reliability of these sensors are not regulated. As sensors become part of the concussion diagnostic process, there is a need for regulation to ensure data are representative of true head kinematics. Preliminary tests were conducted to assess the need for thorough lab testing and public dissemination. The tests concluded that there were widespread differences in sensor performance that must be addressed. The objective of this study was to define and implement laboratory methods as an initial phase in evaluating wearable head impact sensors. Results from these tests under ideal laboratory conditions will be used to determine which sensors exhibit minimal error, adequate for further tests under more realistic conditions. The combination of both testing phases will be used to provide an overall sensor evaluation for both researchers and consumers.

MATERIALS AND METHODS

TEST SETUP

Impact tests were conducted using a custom pendulum impactor with a 15.5 kg anvil and 1.90 m pendulum arm. The total moment of inertia of the pendulum arm and anvil was 72 kg-m^2. A medium NOCSAE headform custom fit with a Hybrid III neck was mounted on a linear slide table with five degrees of freedom (DOF). Tests were performed in both unhelmeted and helmeted conditions. For the unhelmeted condition, a 127 mm diameter and 40 mm thick vinyl-nitrile impactor face was mounted at the end of the anvil. For the helmeted condition, a flat, nylon impactor face measuring 127 mm in diameter and 25 mm thick was used. A large Riddell Speed (Elyria, OH) football helmet without the facemask was worn by the headform throughout helmeted tests.

Figure 1: Pendulum impactor used to test various wearable sensors. The impactor face at the end of the pendulum arm impacts an unhelmeted or helmeted headform connected to a biofidelic neck, mounted to a 5-DOF linear slide table.

Impacts were performed to the front, front boss, rear boss, and rear locations of the headform (Figure 2, Table 1), at targeted head accelerations of 25, 50, 75, and 100 g. The four impact locations were chosen based on their frequency of occurrence in sports[36,37], variability in elevation, equal spacing in azimuth, and ability to result in 25-100 g of linear head acceleration given the test conditions. Facemask impacts were not included due to their high inherent variability and low peak accelerations.[38] The four impact magnitudes were chosen to represent the range of subconcussive and concussive impacts in sports.[22,39,40] It was also found during preliminary tests that error varied with head acceleration for many sensors. To draw more equal comparisons, pendulum angle was varied for each condition to target the four desired head accelerations. To remain consistent between tests, reference values were verified to remain within an average of ±5 g of the target acceleration for each test condition. Each test configuration was repeated four times, totaling 64 tests per sensor.

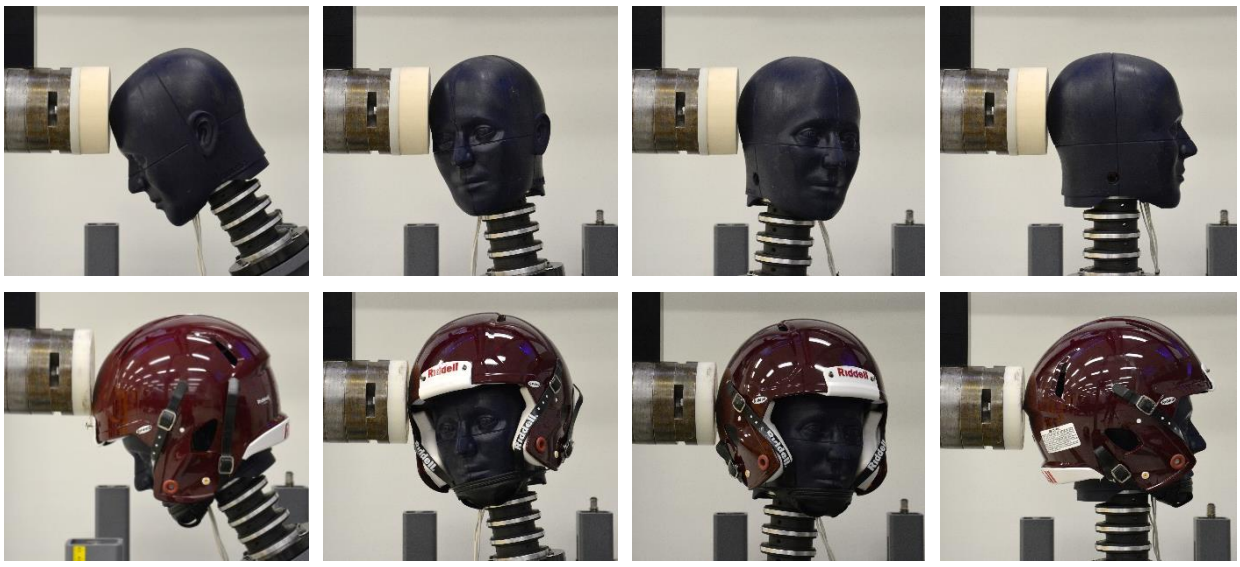

Figure 2: Impact locations for unhelmeted (top) and helmeted (bottom) impacts. From left to right: front, front boss, rear boss, rear.

Table 1: NOCSAE headform locations and rotations on the linear slide table. A centered, upright headform facing the pendulum impactor would have measurements of Y = 40 cm, Ry = 0°, Rz = 0°. Z was obtained by centering the headform or helmet contact point with the center of the impactor.

Condition	Location	Y (cm)	Z (cm)	Ry (deg)	Rz (deg)
Unhelmeted	Front	40	12	30°	0°
	Front Boss	36.5	7	10°	60°
	Rear Boss	42	6	-5°	120°
	Rear	40	6.5	0°	180°
Helmeted	Front	40	6.5	30°	0°
	Front Boss	38	7	10°	60°
	Rear Boss	42	5.5	-5°	120°
	Rear	40	6.5	0°	180°

SENSORS

Six commercially-available wearable head impact sensors were assessed under this protocol (Figure 3, Table 2

Table 2). These include the xPatch developed by X2 Biosystems (Seattle, WA), the Vector Mouth Guard developed by i1 Biometrics (Kirkland, WA), the SIM-G developed by Triax Technologies, the Gforce Tracker (GFT) developed by the company of the same name (Markam, ON), the Shockbox developed by Impakt Protective but now owned by i1 Biometrics (Kirkland, WA), and the HeadsUp Headband developed by Integrated Bionics (Houston, TX). Hereafter, the sensors will be referred to as X2, Vector MG, Triax, GFT, Shockbox, and HeadsUp. Sensor acceleration and velocity measurements were compared to reference headform data provided by three linear accelerometers and three angular rate sensors (6DX Pro 2k-18k 6DOF sensor package DTS, Seal Beach, CA) located in the headform center of mass.

X2 Vector MG Triax GFT Shockbox HeadsUp

Figure 3: Sensors evaluated in this study. Note: images are not identically scaled. Images obtained from Google Images

Table 2: Wearable sensor details. Assessments were performed according to the ability of each sensor.

Sensor	Hardware Last Updated[+]	Components	Peak Headform Outputs*	Time Series Outputs	Output Sampling Rate	Location
X2	Oct 2014	3-axis accelerometer, gyroscope	LA, RV, RA	LA, RV	1000 Hz (RV: 850 Hz)	skin patch
Vector MG	Oct 2015	3-axis accelerometer, gyroscope	LA, RV, RA	LA, RV, RA	5000 Hz	mouth guard
Triax	June 2014	3-axis accelerometer, gyroscope	LA, RV, RA	LA, RV, RA	1000 Hz	headband
GFT	Oct 2015	3-axis accelerometer, gyroscope	LA, RV, RA	LA, RV	3000 Hz (RV: 760 Hz)	helmet, headband
Shockbox	Aug 2014[++]	3-axis accelerometer	LA	n/a	n/a	helmet
HeadsUp	July 2015	3-axis accelerometer	LA**	n/a	n/a	headband

[+] All software and firmware were updated in Oct 2015
* LA = linear acceleration, RV = rotational velocity, RA = rotational acceleration
[++] An older model for Shockbox was tested to be consistent with the model used in Wong et al., 2014 [34]
** HeadsUp measures sensor acceleration, not headform acceleration

X2 was worn as an adhesive skin patch placed behind the right 'ear' of the headform and was tested under both unhelmeted and helmeted conditions. Vector MG is typically worn as a mouth guard, but since the NOCSAE headform is not adapted for mouth guard use, it was firmly adhered to the front of the headform at a 90° angle. The measurement components were placed as close to the proper location as possible, and resultant data instead of component data were used to make the 90° rotation insignificant. Since Vector MG is currently only permitted to be worn during helmeted sports, it was only tested in the helmeted condition. Triax was worn in a headband with the sensor located at the back of the head along the nuchal line and was tested under both unhelmeted and helmeted conditions. GFT has two possible sensor placements: fixed to a headband and adhered to the helmet shell. In the unhelmeted condition, GFT was fixed to a holder in the headband and worn with the sensor located at the back of the head along the nuchal line. In the helmeted condition, the sensor was adhered to the inside, back right side of the helmet shell oriented in the anterior-posterior direction. Shockbox was also adhered to the inside, right side of the helmet shell, oriented in the anterior-posterior direction and only tested in the helmeted condition. HeadsUp was worn in a headband with the sensor located at the back of the head along

the nuchal line. Since the manufacturer currently advertises use for unhelmeted sports, it was tested only under the unhelmeted condition.

DATA ANALYSIS

Linear acceleration and rotational velocity from the headform reference instrumentation were processed using MATLAB R2014a. The reference data were filtered at CFC 1000 for linear acceleration and CFC 155 for rotational acceleration. Peak resultant linear acceleration, rotational velocity, and rotational acceleration values were computed for each impact. Repeatability within each test condition was determined by finding the coefficient of variation (COV) of each kinematic variable. COV is found by dividing the standard deviation in peak values for each test condition by the mean of that test condition. Results were classified as excellent ($COV \leq 3\%$), acceptable ($3 < COV \leq 7\%$), marginal ($7 < COV \leq 10\%$), and poor ($COV > 10\%$) according to the method described by Siegmund et al.[41]

Sensor error was calculated by finding differences in peak values between the reference and wearable sensors. Negative error corresponds to underpredictions by the wearable sensors, whereas positive error corresponds to overpredictions. Average and standard deviations in sensor error were found for each impact location and impact energy. Because the sign of the error was retained, the average can be also known as systematic error, or error that can be improved by a simple correction factor. Standard deviation represents random error, or error that cannot be compensated for through an algebraic expression.

Overall comparisons between sensors and reference were obtained by fitting linear regressions to peak values and obtaining the slope and R^2 coefficient of determination. This was done for each kinematic variable output by each sensor. Linear regressions were also fit for each impact location to describe location-dependent response differences. To equally compare slope and R^2 values, linear regressions were constrained through the origin. As a comparison to reference, the slope is a correlate of systematic error, with values above and below 1.0 indicating under and overprediction, respectively. R^2 is a correlate of random error and gives a measure of the dispersion of the entire set of tests for each sensor.

Significant differences between sensor output and reference values for each test condition were determined through a three-way, repeated measures ANOVA with a post hoc Dunnett test, assuming normal distributions. Independent variables included sensor name, location, impact energy, and all interaction terms, while the dependent variable was sensor error. HeadsUp and Shockbox were removed from analysis due to lack of data in some test conditions. All remaining sensors were included together in the analysis, and one ANOVA and post hoc test was performed per kinematic variable. The results of the ANOVA gave least squares (LS) mean error and 95% confidence intervals on the least squares mean within each effect and interaction term. The post hoc Dunnett tests compared LS-mean error at each condition to zero, and was performed on the interaction term between sensor name, location, and impact energy. Since sensor results were balanced, decision limits were constant for all sensors and based on overall variance. Statistical significance was concluded when $p \leq 0.05$.

Planned contrasts in specific effects and interaction terms within the ANOVA described above were used to make additional conclusions on subsets of the data. Planned contrasts in the 'sensor name' effect tested the hypothesis that unhelmeted and helmeted conditions of the same sensor had equal LS-mean errors. Planned contrasts in the interactions between sensor and location and between sensor and impact energy tested the hypotheses that for each sensor, the LS-mean error for each location or impact energy were equal. Statistical significance was concluded when $p \leq 0.05$. All statistical analyses were performed with JMP 12.

For the sensors that also output time series data, comparisons were made at each time point rather than on peak values. Since triggering thresholds for the start of the impact varied for each sensor compared to reference, the curves required systematic alignment. Sensor curves were iteratively time-shifted along references curves, and root mean square (RMS) error (Equation 1) between the sensor and reference was found at each iteration. Proper alignment was concluded at the iteration with minimum RMS error.

Equation 1: Root mean square error calculation for an entire time series. Here, x_{ref} is the kinematic value for the reference, x_s is the kinematic value for the wearable sensor, and n is the number of points in the time series. The squared error is summed over all time steps.

$$RMS = \sqrt{\frac{\sum\left(x_{ref} - x_s\right)^2}{n}}$$

To equally compare between test conditions, the minimum RMS error at a given test condition was normalized with respect to the reference peak. To graphically represent the results for each test condition, sensor and reference curves were each averaged. Corridors were defined for sensor and reference averages by the average ± one standard deviation at each test condition. Average and standard deviations of normalized RMS error (NRMSE) were also calculated for each test condition.

Significant differences in NRMSE from zero were tested similarly to sensor error using a three-way, repeated measures ANOVA, a post hoc Dunnett test, and planned contrasts. One ANOVA and post hoc test was performed per kinematic variable. The post hoc Dunnett tests compared LS-mean NRMSE at each condition to zero, and was performed on the interaction term between sensor name, location, and impact energy. Planned contrasts in the 'sensor name' effect tested the hypothesis that unhelmeted and helmeted conditions of the same sensor had equal LS-mean NRMSE. Planned contrasts in the interactions between sensor and location and between sensor and impact energy tested the hypotheses that for each sensor, the LS-mean NRMSE for each location or impact energy were equal. Statistical significance was concluded when $p \leq 0.05$.

RESULTS

REFERENCE

Linear acceleration reference values for all tests were verified to remain within ±5 g of the targeted acceleration. For further analysis of repeatability, the coefficient of variation was found for each test condition (Table 3). Note that COV was calculated for each condition across tests for all six sensors and does not represent variations within one test series. For each individual test series, variation was lower than the results shown below. Overall, there was greater repeatability with the unhelmeted compared to the helmeted tests, and for the rotational velocity values compared to the other two kinematic variables. Most test conditions exhibited excellent (≤ 3%) to acceptable (3 < COV ≤ 7%) repeatability. Exceptions to this mainly occurred in the targeted 25g tests for the helmeted condition in linear acceleration. The worst repeatability was found in rotational acceleration for the helmeted rear tests, where COV was poor (> 10%) for three of the four impact magnitudes. However, if COV was calculated for individual test series, results would remain less than 6% for all impact magnitudes.

Table 3: Coefficients of variation (COV) for reference values at each test condition. LA, RV, and RA represent linear acceleration, rotational velocity, and rotational acceleration, respectively. U and H represent unhelmeted and helmeted conditions.

Location	**Target LA**	**LA (%)**		**RV (%)**		**RA (%)**	
		U	*H*	*U*	*H*	*U*	*H*
Front	**25**	4.17	5.41	2.87	1.69	6.14	4.07
	50	2.44	3.22	1.62	2.60	4.63	6.73
	75	2.81	2.75	1.38	3.81	3.62	7.34
	100	2.94	4.90	1.29	2.11	3.58	5.41
Front Boss	**25**	9.98	5.06	2.13	2.35	6.68	4.37
	50	2.93	4.80	0.77	3.43	3.73	2.35
	75	3.52	3.14	1.14	2.82	5.31	3.39
	100	1.31	2.74	1.87	3.63	4.87	4.19
Rear Boss	**25**	6.01	12.42	1.39	1.48	6.32	6.39
	50	3.48	9.05	0.41	3.71	2.87	3.74
	75	1.07	3.63	0.74	3.29	1.72	4.03
	100	1.35	3.66	1.09	4.57	1.62	8.85
Rear	**25**	8.14	16.98	1.80	4.04	8.48	13.57
	50	5.24	8.59	0.57	4.30	7.83	14.90
	75	1.06	4.13	1.24	5.01	5.07	7.84
	100	2.11	2.34	0.93	4.46	2.31	15.43

WEARABLE SENSORS

Results of the ANOVA gave overall comparisons in least squares mean sensor error and NRMSE for each sensor in the analysis. Separate results were given for each kinematic variable.

The LS-mean in sensor error does not give any representation to the random error component for each sensor. Rather, the LS-means and 95% confidence intervals give information on the systematic under or overpredictions of the reference, adjusted for other effects in the model. Graphical results of LS-mean sensor error and confidence intervals are given for each sensor in both helmeted and unhelmeted conditions (Figure 4). Note that Vector MG was not tested under an unhelmeted condition, and GFT does not output rotational acceleration.

In linear acceleration, X2 displayed the least sensor error in both unhelmeted and helmeted conditions compared to other sensors. No significant difference was found between its two test conditions. Triax was the second best sensor in terms of LS-mean error in both unhelmeted and helmeted conditions. Its unhelmeted condition underpredicted the reference overall, while the helmeted condition overpredicted, resulting in significant differences between the two conditions. Vector MG displayed the third least LS-mean error and overpredicted the reference overall. GFT exhibited the largest errors especially in the helmeted condition, resulting in significant differences between the two conditions.

Rotational velocity results exhibited slightly different trends than linear acceleration. X2 still underpredicted the references and showed the least error. However, the second least error was exhibited by Vector MG which underpredicted the reference. Following Vector MG was the helmeted GFT tests which also underpredicted the reference. Fourth were the Triax conditions, and finally unhelmeted GFT. Here, only GFT displayed significance between the unhelmeted and helmeted conditions.

Rotational acceleration LS-mean results showed Vector MG with the least error, closely followed by helmeted Triax tests and X2. The greatest error was shown in unhelmeted Triax which was found to be significantly different from the helmeted condition. Notice also that errors for all

sensors deviate largely from zero in rotational acceleration, while most sensors closely surround zero for the other kinematic variables.

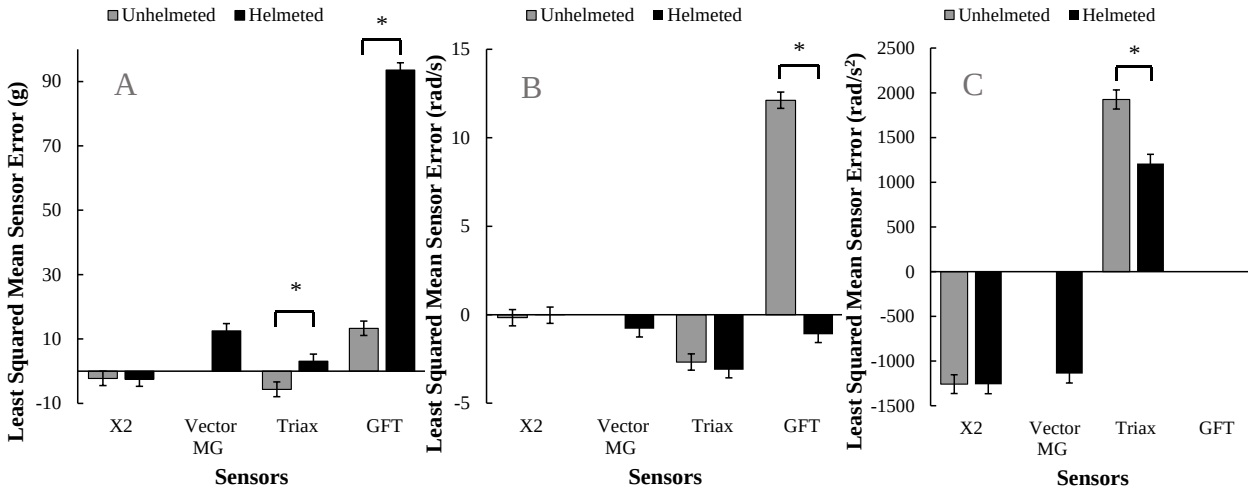

Figure 4: Least-squares mean sensor error in linear acceleration (A), rotational velocity (B), and rotational acceleration (C). Error bars denote 95% confidence intervals in LS-mean error. The asterisks denote significance between test conditions as determined by planned contrasts. Significance is only shown to compare unhelmeted and helmeted conditions for each sensor.

Graphical results of LS-mean NRMSE and confidence intervals are given for each sensor in both helmeted and unhelmeted conditions (Figure 5). Note that Vector MG was not tested under an unhelmeted condition, and neither X2 nor GFT output rotational acceleration time series. These results give information about the systematic NRMSE and are always positive because of the nature of RMS error calculations.

In linear acceleration, X2 displayed the least error and no significant differences between test conditions. Following X2 were Vector MG, Triax, and GFT, in that order. The unhelmeted conditions performed better than helmeted for both Triax and GFT, resulting in significant differences in conditions for each sensor.

Rotational velocity exhibited a similar trend. X2 and Vector MG had the least NRMSE. However, they were first followed by helmeted GFT and then both Triax conditions. Unhelmeted GFT displayed the greatest error. For rotational velocity, the helmeted conditions in Triax and GFT performed better than unhelmeted, although there was only a significant difference in GFT.

In rotational acceleration, Vector MG displayed the least error, followed by helmeted and unhelmeted Triax. A significant difference was found between the two Triax conditions.

Since these values were normalized to peak reference, they can also be compared across kinematic variables. X2, Vector MG, Triax, and helmeted GFT all experienced the least error in rotational velocity compared to the other variables. Only unhelmeted GFT demonstrated the least error in linear acceleration.

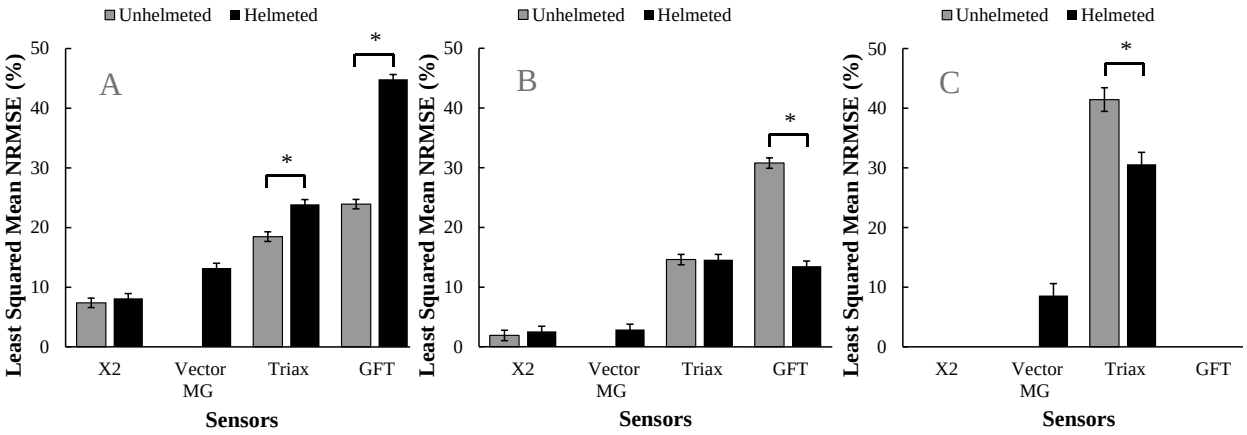

Figure 5: Least-squares mean normalized RMS error in linear acceleration (A), rotational velocity (B), and rotational acceleration (C). Error bars denote 95% confidence intervals in LS-mean NRMSE. The asterisks denote significance between test conditions as determined by planned contrasts. Significance is only shown to compare unhelmeted and helmeted conditions for each sensor.

xPatch, X2 Biosystems

Unhelmeted

X2 successfully recorded all 64 unhelmeted impacts. Systematic and random error for each test condition remained low for linear acceleration and rotational velocity. X2 slightly underpredicted the reference at high impact magnitudes in linear acceleration. Rotational acceleration consistently underpredicted the reference for all test conditions (Table 4).

Table 4: Average (SD) sensor error for unhelmeted X2 tests. Significance, denoted by asterisks, only occurred in rotational acceleration at high-energy impacts to the front boss, rear boss, and rear locations. Column headings in peak linear acceleration represent the targeted values, while column headings for the other variables are peak reference averages for each impact energy.

	Error in Peak Linear Acceleration (g)							
	25		**50**		**75**		**100**	
Front	2.1	(0.1)	2.6	(0.4)	1.8	(1.7)	-4.6	(1.0)
Front Boss	3.8	(0.2)	3.1	(0.1)	-2.0	(1.3)	-6.3	(2.1)
Rear Boss	-0.5	(0.6)	-4.3	(0.7)	-9.3	(0.5)	-12.9	(0.9)
Rear	0.1	(0.2)	-1.6	(0.1)	-2.2	(0.9)	-5.7	(1.0)

	Error in Peak Rotational Velocity (rad/s)							
	12		**22**		**31**		**37**	
Front	-0.3	(0.1)	-0.4	(0.1)	-0.7	(0.0)	-0.9	(0.1)
Front Boss	-0.1	(0.1)	-0.2	(0.1)	-0.3	(0.1)	-0.4	(0.2)
Rear Boss	0.1	(0.1)	0.4	(0.1)	0.5	(0.1)	0.9	(0.1)
Rear	-0.3	(0.1)	-0.6	(0.1)	0.2	(1.8)	-0.6	(0.1)

	Error in Peak Rotational Acceleration (rad/s/s)							
	1377		**2538**		**3686**		**4824**	
Front	-240.2	(48.5)	-130.5	(120.1)	-227.0	(90.1)	-322.5	(160.0)
Front Boss	-658.9	(73.6)	-1425.9	(70.7)*	-2047.4	(25.3)*	-2738.5	(134.0)*
Rear Boss	-747.3	(69.6)	-1451.5	(219.0)*	-2235.7	(273.5)*	-3036.8	(311.9)*
Rear	-337.6	(54.6)	-975.1	(111.0)*	-1376.9	(191.7)*	-2168.3	(134.0)*

According to the linear regressions for each location, R^2 values remained above 0.93 for all kinematic variables (Table 5, Figure 6). Although the overall R^2 values in linear acceleration and rotational velocity remained high, overall R^2 for rotational acceleration was 0.612. Slopes of the linear regressions for linear acceleration and rotational velocity remained within 13% of 1.0 (Table 6). In rotational acceleration, the slope reached 2.14 in front boss and 1.65 overall.

Table 5: R^2 values from linear regressions constrained through the origin for unhelmeted X2. LA, RV, and RA signify linear acceleration, rotational velocity, and rotational acceleration, respectively.

	LA	**RV**	**RA**
Front	0.99	1.00	0.98
Front Boss	0.98	1.00	0.97
Rear Boss	1.00	1.00	0.95
Rear	1.00	0.99	0.93
Total	0.98	1.00	0.61

Table 6: Slopes from linear regressions constrained through the origin for unhelmeted X2. LA, RV, and RA signify linear acceleration, rotational velocity, and rotational acceleration, respectively.

	LA	RV	RA
Front	1.01	1.03	1.10
Front Boss	1.03	1.01	2.14
Rear Boss	1.13	0.98	1.95
Rear	1.05	1.01	1.75
Total	1.05	1.01	1.65

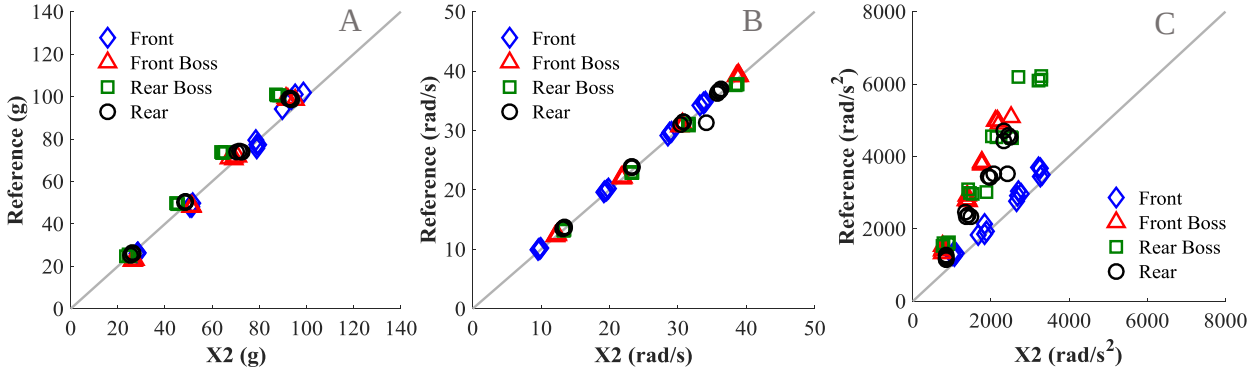

Figure 6: Peak reference values versus peak unhelmeted X2 values in linear acceleration (A), rotational velocity (B), and rotational acceleration (C). A 1:1 diagonal is drawn on each graph to visually show the amount of overprediction (points below line) and underprediction (points above line) of the reference.

The results from planned contrasts indicated significant differences in impact energies for linear acceleration, no significance in rotational velocity, and significant differences in both location and energy for rotational acceleration ($p<0.05$).

For unhelmeted tests, NRMSE never exceeded 8.7% in linear acceleration and 3.6% in rotational velocity (Table 7). For all test conditions, qualitative comparisons between sensor time series and reference show close similarities in curve shapes (Figure A-1, Figure A-2).

Table 7: Average (SD) NRMSE for unhelmeted X2 tests. Significance, denoted by asterisks, in linear acceleration was found in the front boss, rear boss, and rear locations at multiple impact energies despite the close similarities in curve shapes. There was no significance in rotational velocity. Column headings in peak linear acceleration represent the targeted values, while column headings in rotational velocity are peak reference averages for each impact energy.

	NRMSE in Peak Linear Acceleration (%)			
	25	**50**	**75**	**100**
Front	6.5 (0.2)	6.7 (0.2)	6.7 (0.6)	6.4 (0.6)
Front Boss	7.9 (0.6)*	7.4 (0.1)*	7.1 (0.2)	7.5 (0.2)*
Rear Boss	7.5 (0.2)*	7.1 (0.2)	7.4 (0.2)*	6.7 (0.1)
Rear	8.2 (0.2)*	8.6 (0.3)*	8.7 (0.2)*	7.9 (0.3)*

	NRMSE in Peak Rotational Velocity (%)			
	12	**22**	**31**	**37**
Front	1.5 (0.4)	1.3 (0.5)	1.2 (0.5)	1.6 (0.2)
Front Boss	1.9 (0.5)	1.9 (0.2)	2.0 (0.1)	3.2 (1.9)
Rear Boss	1.4 (0.2)	1.9 (0.1)	2.3 (0.1)	2.6 (0.1)
Rear	1.4 (0.3)	1.2 (0.4)	3.6 (4.4)	1.5 (0.2)

The results from planned contrasts indicated no significant differences in location or impact energy for linear acceleration or rotational velocity according to NRMSE ($p<0.05$).

Helmeted

Helmeted X2 successfully recorded all 64 impacts. Systematic and random error for each test condition still remained low for linear acceleration and rotational velocity, although they were higher than in the unhelmeted condition. Peak systematic error in linear acceleration increased with impact energy, underpredicted the reference in the front boss and rear boss locations, and overpredicted in the other locations. Systematic errors remained fairly constant in rotational velocity. Rotational acceleration systematic and random error increased with impact energy and consistently underpredicted the reference (Table 8).

Table 8: Average (SD) sensor error for helmeted X2 tests. Significance, denoted by asterisks, only occurred in rotational acceleration for the front boss and rear boss locations at multiple impact energies. Column headings in peak linear acceleration represent the targeted values, while column headings for the other variables are peak reference averages for each impact energy.

Error in Peak Linear Acceleration (g)								
	25		**50**		**75**		**100**	
Front	-0.1	(1.5)	3.1	(0.6)	5.1	(0.8)	3.2	(2.1)
Front Boss	-2.3	(0.1)	-11.4	(1.0)	-16.2	(3.1)	-18.9	(1.3)
Rear Boss	-1.4	(2.4)	-6.4	(4.1)	-9.1	(4.4)	-12.7	(3.9)
Rear	3.4	(0.9)	6.2	(4.7)	5.1	(2.7)	12.7	(15.7)

Error in Peak Rotational Velocity (rad/s)								
	12		**20**		**28**		**33**	
Front	-0.6	(0.2)	-0.9	(0.1)	-0.9	(0.2)	2.9	(6.9)
Front Boss	0.0	(0.1)	0.0	(0.1)	0.3	(0.1)	0.1	(0.2)
Rear Boss	0.2	(0.2)	0.4	(0.1)	0.6	(0.3)	0.4	(0.3)
Rear	-0.2	(0.0)	-0.5	(0.2)	-1.2	(0.2)	-1.2	(0.2)

Error in Peak Rotational Acceleration (rad/s/s)								
	1587		**3060**		**4205**		**5272**	
Front	-191.3	(10.5)	-336.6	(22.8)	-536.1	(101.5)	-730.5	(144.7)
Front Boss	-1276.8	(83.3)	-3015.7	(217.1)	-3631.3	(627.2)	-4564.8	(244.3)
Rear Boss	-223.5	(147.0)*	-1577.2	(184.3)*	-1420.6	(453.3)*	-1608.1	(274.9)*
Rear	-279.7	(45.8)	-358.8	(54.7)*	-233.1	(137.7)*	-187.4	(121.9)*

According to the linear regressions, helmeted X2 correlated with the reference better for rotational velocity than for the other kinematic variables (Table 9, Figure 7). When evaluating each location separately, the R^2 values from the linear regressions remained above 0.94 for linear acceleration, 0.82 for rotational velocity, and 0.79 for rotational acceleration. However, the overall R^2 value for linear acceleration was 0.86 and for rotational acceleration was 0.127. Note the front location in rotational velocity had one distinct outlier (Figure 7B) that is caused by an erroneous first data point in the time series. If the correct peak was calculated, the R^2 value for the front location would be 0.991, and the overall R^2 would be 0.995. Slopes of the linear regressions for linear acceleration and rotational velocity remained within 25% of 1.0 individually and 2% overall (Table 10). In rotational acceleration, the slope reached 2.99 in front boss and 1.41 overall.

Table 9: R^2 values from linear regressions constrained through the origin for helmeted X2. LA, RV, and RA signify linear acceleration, rotational velocity, and rotational acceleration, respectively.

	LA	RV	RA
Front	1.00	0.83	0.99
Front Boss	0.99	1.00	0.80
Rear Boss	0.98	1.00	0.83
Rear	0.94	1.00	0.98
Total	0.86	0.95	0.13

Table 10: Slopes from linear regressions constrained through the origin for helmeted X2. LA, RV, and RA signify linear acceleration, rotational velocity, and rotational acceleration, respectively.

	LA	RV	RA
Front	0.96	0.96	1.22
Front Boss	1.25	0.99	2.99
Rear Boss	1.13	0.98	1.42
Rear	0.90	1.03	1.07
Total	1.02	0.99	1.41

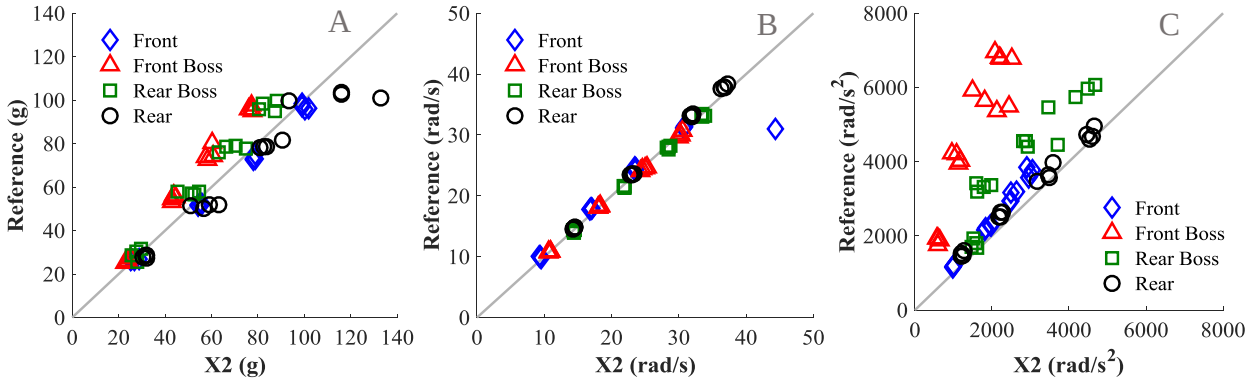

Figure 7: Peak reference values versus peak helmeted X2 values in linear acceleration (A), rotational velocity (B), and rotational acceleration (C). A 1:1 diagonal is drawn on each graph to visually show the amount of overprediction (points below line) and underprediction (points above line) of the reference.

The results from the planned contrasts indicated significant differences in location for linear acceleration, no significance for rotational velocity, and significant differences in both location and energy for rotational acceleration ($p<0.05$).

For helmeted X2 tests, NRMSE never exceeded 12.6% in linear acceleration and 5.0% in rotational velocity (Table 11). The largest differences in linear acceleration occurred in the rear boss and rear

locations which exhibited spikes in acceleration just before the peak (Figure A-3). Rotational velocity curves were very similar between X2 and reference, except for the occasional erroneous first data point in some test conditions (Figure A-4).

Table 11: Average (SD) NRMSE for helmeted X2 tests. Significance, denoted by asterisks, in linear acceleration was found in the low-energy front boss impact, and all rear boss and rear impacts. There was no significance in rotational velocity. Column headings in peak linear acceleration represent the targeted values, while column headings for rotational velocity are peak reference averages for each impact energy.

	NRMSE in Peak Linear Acceleration (%)			
	25	**50**	**75**	**100**
Front	6.3 (0.3)	6.5 (0.3)	5.3 (0.9)	6.6 (0.2)
Front Boss	7.6 (0.3)*	6.5 (0.2)	6.9 (0.7)	6.6 (0.4)
Rear Boss	12.5 (5.9)*	9.6 (0.8)*	9.8 (2.9)*	8.2 (0.9)*
Rear	9.5 (1.0)*	9.5 (1.0)*	9.3 (1.9)*	9.5 (1.8)*

	NRMSE in Peak Rotational Velocity (%)			
	12	**22**	**31**	**37**
Front	1.6 (0.5)	1.9 (0.2)	2.0 (0.4)	4.9 (5.9)
Front Boss	1.4 (0.2)	1.6 (0.1)	2.1 (0.4)	2.7 (0.5)
Rear Boss	3.2 (0.3)	4.4 (0.5)	3.3 (0.6)	3.5 (0.9)
Rear	1.6 (0.5)	3.1 (0.8)	2.3 (0.3)	1.7 (0.6)

The results from the planned contrasts only showed significance in location for linear acceleration according to NRMSE ($p<0.05$).

Vector Mouth Guard, i1 Biometrics

Vector MG successfully recorded all 64 impacts under helmeted conditions. In linear acceleration, systematic and random error remained low for the front and rear boss impacts. For front boss and rear impacts, systematic error increased with impact energy such that Vector MG largely overpredicted the reference. In rotational velocity, systematic and random error remained relatively constant for all locations and impact energies. In rotational acceleration, systematic and random error increased with impact energy and consistently underpredicted the reference (Table 12).

Table 12: Average (SD) sensor error for Vector MG tests. Significance, denoted by asterisks, was determined for the high-energy front boss and rear locations in linear acceleration and the front boss and rear boss locations in rotational acceleration. There was no significance in rotational velocity. Column headings in peak linear acceleration represent the targeted values, while column headings for the other variables are peak reference averages for each impact energy.

Error in Peak Linear Acceleration (g)								
	25		**50**		**75**		**100**	
Front	4.0	(0.4)	2.4	(1.4)	-0.5	(2.8)	5.4	(1.2)
Front Boss	14.2	(2.2)	36.5	(1.2)*	43.3	(4.8)*	44.5	(10.6)*
Rear Boss	-3.0	(1.5)	-8.0	(0.6)	-7.6	(0.8)	-11.4	(1.3)
Rear	9.6	(0.5)	15.8	(2.4)	23.4	(1.0)*	31.9	(1.0)*

Error in Peak Rotational Velocity (rad/s)								
	12		**20**		**28**		**33**	
Front	-0.5	(0.2)	-1.0	(0.1)	-0.9	(0.1)	-0.9	(0.1)
Front Boss	-0.2	(0.0)	-0.7	(0.1)	-0.8	(0.1)	-1.5	(0.1)
Rear Boss	-0.5	(0.1)	-0.3	(0.1)	-0.5	(0.1)	-0.3	(0.2)
Rear	-0.5	(0.1)	-0.8	(0.3)	-1.8	(1.0)	-1.7	(0.2)

Error in Peak Rotational Acceleration (rad/s/s)								
	1587		**3060**		**4205**		**5272**	
Front	-252.6	(18.0)	-481.8	(51.6)	-690.2	(99.7)	-791.7	(114.3)
Front Boss	-842.6	(49.7)	-2105.2	(116.5)*	-2885.5	(193.1)*	-3490.6	(72.7)*
Rear Boss	-519.7	(82.5)	-969.3	(76.4)*	-1320.1	(125.8)*	-1833.3	(220.9)*
Rear	-322.6	(48.9)	-413.7	(16.6)	-527.3	(165.0)	-813.4	(103.3)

According to linear regressions, Vector MG correlated with the reference in each location for all three kinematic variables, with R^2 above 0.96 (Table 13, Figure 8). However, overall R^2 values were 0.70 for linear acceleration and 0.74 for rotational acceleration. Slopes of the linear regressions for all kinematic variables remained within 3% of 1.0 individually but were 0.80 and 1.47 for linear and rotational acceleration overall (Table 14).

Table 13: R^2 values from linear regressions constrained through the origin for helmeted Vector MG. LA, RV, and RA signify linear acceleration, rotational velocity, and rotational acceleration, respectively.

	LA	**RV**	**RA**
Front	0.99	1.00	0.99
Front Boss	0.97	1.00	0.99
Rear Boss	1.00	1.00	0.99
Rear	1.00	1.00	0.99
Total	0.70	1.00	0.73

Table 14: Slopes from linear regressions constrained through the origin for helmeted Vector MG. LA, RV, and RA signify linear acceleration, rotational velocity, and rotational acceleration, respectively.

	LA	RV	RA
Front	0.96	1.04	1.28
Front Boss	0.65	1.04	2.04
Rear Boss	1.13	1.01	1.44
Rear	0.76	1.05	1.20
Total	0.80	1.04	1.47

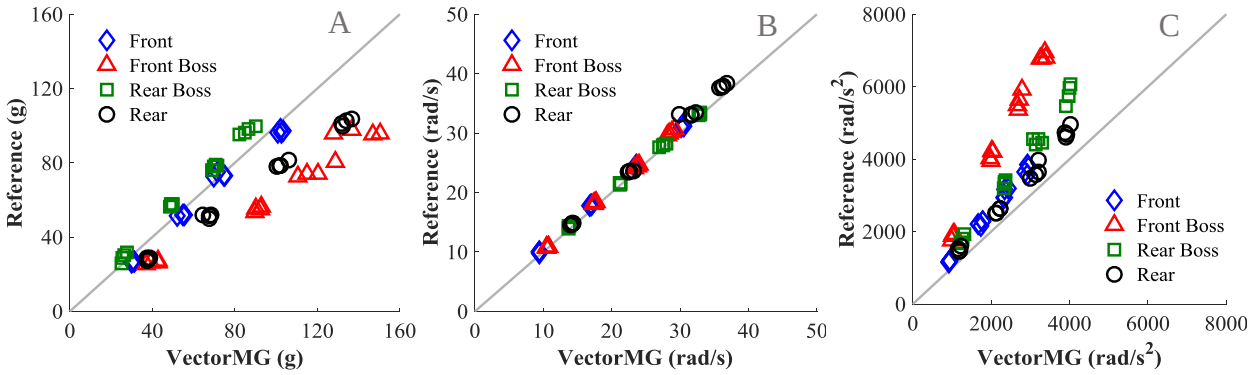

Figure 8: Peak reference values versus peak helmeted Vector MG values in linear acceleration (A), rotational velocity (B), and rotational acceleration (C). A 1:1 diagonal is drawn on each graph to visually show the amount of overprediction (points below line) and underprediction (points above line) of the reference.

The results from planned contrasts indicated significant differences in location and impact energies for linear and rotational acceleration. No significance was found among conditions in rotational velocity ($p<0.05$).

Average NRMSE ranged from 4.3% to 22.7% in linear acceleration, 1.7% to 4.8% in rotational velocity, and 6.6% to 11.5% in rotational acceleration (Table 15). Qualitative comparisons between curve shapes showed a wider peak in Vector MG for the front and rear locations in linear acceleration (Figure A-5). Front boss and rear locations also overpredicted the reference. Rotational velocity and acceleration curves were very similar between Vector MG and the reference, although rotational acceleration in the sensor overpredicted the reference in most tests (Figure A-6, Figure A-7).

Table 15: Average (SD) NRMSE for helmeted Vector MG tests. Significance, denoted by asterisks, in linear acceleration was found almost all tests except those to the rear boss at the 25, 50, and 75 g energy levels. There was no significance in rotational velocity or acceleration. Column headings in peak linear acceleration represent the targeted values, while column headings for the other variables are peak reference averages for each impact energy.

NRMSE in Peak Linear Acceleration (%)								
	25		**50**		**75**		**100**	
Front	17.6	(0.6)*	17.5	(0.3)*	16.9	(0.2)*	16.1	(0.2)*
Front Boss	11.7	(0.6)*	10.9	(0.4)*	9.6	(0.5)*	8.7	(0.8)*
Rear Boss	4.6	(0.2)	4.3	(0.1)	6.7	(1.6)	7.5	(1.0)*
Rear	20.0	(0.1)*	22.7	(4.1)*	19.2	(1.1)*	17.2	(1.0)*

NRMSE in Peak Rotational Velocity (%)								
	12		**20**		**28**		**33**	
Front	2.5	(0.4)	2.4	(0.2)	2.4	(0.1)	2.3	(0.1)
Front Boss	2.6	(0.4)	3.7	(0.3)	3.9	(0.2)	4.0	(0.3)
Rear Boss	1.7	(0.1)	2.2	(0.1)	3.3	(1.0)	4.8	(1.0)
Rear	1.7	(0.1)	4.1	(2.7)	2.2	(0.6)	3.1	(1.8)

NRMSE in Peak Rotational Acceleration (%)								
	1587		**3060**		**4205**		**5272**	
Front	11.5	(0.8)	8.8	(0.3)	8.5	(0.6)	8.7	(0.2)
Front Boss	8.8	(0.5)	8.4	(0.1)	8.4	(0.2)	8.6	(0.2)
Rear Boss	8.0	(0.5)	7.1	(0.1)	8.3	(1.3)	8.7	(0.6)
Rear	9.2	(0.6)	11.1	(4.0)	6.6	(1.2)	7.0	(2.1)

The results from planned contrasts only indicated significant differences in location for linear acceleration according to NRMSE. There were no significant differences in condition for the other two kinematic variables ($p<0.05$).

SIM-G, Triax Technologies

Unhelmeted

Triax failed to record two lower-magnitude front impacts in the unhelmeted condition. No reasonable explanations for these missed impacts can be offered. For the recorded impacts, sensor errors in linear acceleration were widely variable. The least systematic error was exhibited by the front boss location at lower impact energies. The most random error was exhibited in the front location at higher energies. Systematic and random error in rotational velocity were relatively low throughout all tests, although did increase slightly with impact energy. Rotational acceleration

exhibited reasonable systematic and random error in front boss and rear boss, although it largely overpredicted the reference in the front and rear, especially at high impact energies (Table 16).

Table 16: Average (SD) sensor error for unhelmeted Triax tests. Various test conditions in all three kinematic variables were found to contain sensor error significantly different from zero, as denoted by asterisks. These significances occurred most often at the highest impact energies or in the rear location. Column headings in peak linear acceleration represent the targeted values, while column headings for the other variables are peak reference averages for each impact energy.

	Error in Peak Linear Acceleration (g)							
	25		**50**		**75**		**100**	
Front	-1.0	(7.4)	-20.5	(17.2)	-25.5	(14.1)*	-47.9	(13.4)*
Front Boss	2.9	(4.4)	-2.8	(5.7)	-11.2	(0.3)	-33.0	(0.6)*
Rear Boss	14.1	(6.3)	21.3	(3.6)*	1.2	(1.6)	-21.0	(1.0)*
Rear	33.8	(17.6)*	26.3	(1.8)*	1.4	(10.6)	-28.2	(7.3)*

	Error in Peak Rotational Velocity (rad/s)							
	12		**22**		**31**		**37**	
Front	-1.8	(0.1)	-2.8	(0.6)	-2.4	(1.4)	-5.4	(0.1)*
Front Boss	-2.1	(0.1)	-3.5	(0.2)	-3.8	(0.3)	-5.9	(1.9)*
Rear Boss	-0.7	(0.6)	-2.6	(0.2)	-4.7	(0.7)*	-6.6	(0.1)*
Rear	0.9	(0.4)	3.8	(0.2)	-0.6	(0.6)	-4.6	(1.6)*

	Error in Peak Rotational Acceleration (rad/s/s)							
	1377		**2538**		**3686**		**4824**	
Front	-526.8	(499.3)	-557.3	(885.3)	2501.5	(813.6)*	1244.6	(473.9)*
Front Boss	-271.7	(98.3)	-642.6	(76.2)	-913.0	(26.6)*	-864.5	(63.6)
Rear Boss	437.6	(380.8)	409.4	(101.8)	540.3	(168.8)	2112.3	(630.0)*
Rear	2076.6	(745.9)*	5814.6	(299.6)*	9502.2	(729.2)*	9260.9	(503.9)*

From linear regressions, it can be seen that unhelmeted Triax had lowest error in rotational velocity compared to the other kinematic variables (Table 17, Figure 9). In linear acceleration, the front boss location had the most correlation to reference with R^2 of 0.84. In rotational acceleration, the front boss, rear boss, and rear location all had high correlation with R^2 above 0.92, however the overall correlation was negative. Slopes of the linear regressions for all kinematic variables ranged from 2-60% of 1.0 individually (Table 18). However overall, linear acceleration and rotational velocity had low systematic differences with slopes of 1.06 and 1.12.

Table 17: R^2 values from linear regressions constrained through the origin for unhelmeted Triax. LA, RV, and RA signify linear acceleration, rotational velocity, and rotational acceleration, respectively.

	LA	RV	RA
Front	0.37	0.98	0.39
Front Boss	0.84	0.99	0.99
Rear Boss	0.64	0.98	0.93
Rear	0.09	0.87	0.92
Total	0.25	0.93	-0.56

Table 18: Slopes from linear regressions constrained through the origin for unhelmeted Triax. LA, RV, and RA signify linear acceleration, rotational velocity, and rotational acceleration, respectively.

	LA	RV	RA
Front	1.55	1.14	0.65
Front Boss	1.27	1.17	1.25
Rear Boss	0.97	1.17	0.79
Rear	0.88	1.02	0.30
Total	1.06	1.12	0.46

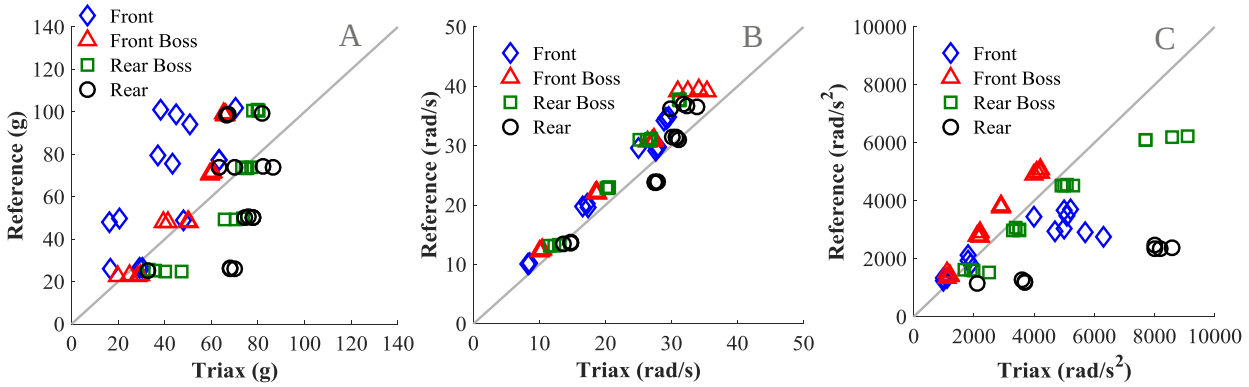

Figure 9: Peak reference values versus peak unhelmeted Triax values in linear acceleration (A), rotational velocity (B), and rotational acceleration (C). A 1:1 diagonal is drawn on each graph to visually show the amount of overprediction (points below line) and underprediction (points above line) of the reference.

The results from planned contrasts indicated significant differences in location and impact energies for all three kinematic variables ($p<0.05$).

For unhelmeted tests, average NRMSE ranged from 11.0% to 34.6% in linear acceleration, 6.9% to 27.2% in rotational velocity, and 8.0% to 130.7% in rotational acceleration (Table 19). Qualitatively, similarities exist between Triax and the reference in curve shapes for all three kinematic variables. However, the front and rear locations had large variations between tests as

illustrated by the wide corridors. Also, the rear location in rotational acceleration greatly overpredicted the reference (Figure A-8, Figure A-9, Figure A-10).

Table 19: Average (SD) NRMSE for unhelmeted Triax tests. Significance, denoted by asterisks, was concluded for almost every test conditions for all three kinematic variables. Exceptions include low-energy front impacts in rotational velocity, and lower energy front and front boss impacts in rotational acceleration. Column headings in peak linear acceleration represent the targeted values, while column headings for the other variables are peak reference averages for each impact energy.

NRMSE in Peak Linear Acceleration (%)								
	25		**50**		**75**		**100**	
Front	14.6	(10.6)*	16.9	(11.9)*	21.5	(5.5)*	20.7	(4.5)*
Front Boss	15.5	(0.9)*	13.3	(1.0)*	11.8	(0.4)*	11.8	(0.5)*
Rear Boss	24.4	(3.4)*	18.3	(1.5)*	11.0	(0.3)*	11.7	(1.4)*
Rear	34.6	(10.2)*	21.8	(4.6)*	19.0	(5.5)*	18.2	(2.9)*

NRMSE in Peak Rotational Velocity (%)								
	12		**22**		**31**		**37**	
Front	7.7	(5.1)	6.9	(4.7)	19.7	(2.6)*	17.7	(0.8)*
Front Boss	11.1	(0.2)*	11.3	(0.0)*	11.4	(0.1)*	12.9	(0.4)*
Rear Boss	15.7	(3.8)*	14.4	(0.3)*	15.8	(2.9)*	12.8	(0.3)*
Rear	16.0	(1.2)*	12.8	(0.4)*	20.4	(2.0)*	27.2	(0.7)*

NRMSE in Peak Rotational Acceleration (%)								
	1377		**2538**		**3686**		**4824**	
Front	8.0	(5.4)	9.8	(7.7)	51.9	(8.6)*	40.8	(4.0)*
Front Boss	10.1	(0.5)	11.9	(0.5)	15.2	(0.8)	16.7	(2.0)*
Rear Boss	35.3	(13.6)*	21.4	(1.4)*	27.1	(2.6)*	34.2	(1.5)*
Rear	64.3	(15.3)*	84.4	(6.1)*	130.7	(12.5)*	101.6	(7.7)*

The results from planned contrasts according to NRMSE indicated significant differences in location and impact energies for all three kinematic variables ($p<0.05$).

Helmeted

Triax recorded at 64 impacts in the helmeted condition. Similar to unhelmeted tests, the helmeted Triax showed large variations in systematic error for all test conditions in linear and rotational acceleration. Linear acceleration also exhibited large random error in the front and rear locations. Rotational velocity values showed high systematic error only in the rear location (Table 20).

Table 20: Average (SD) sensor error for helmeted Triax tests. Various test conditions in all three kinematic variables were found to contain sensor error significantly different from zero. Column headings in peak linear acceleration represent the targeted values, while column headings for the other variables are peak reference averages for each impact energy.

Error in Peak Linear Acceleration (g)								
	25		**50**		**75**		**100**	
Front	17.0	(18.7)	5.9	(6.8)	-12.7	(12.8)	-47.3	(15.9)*
Front Boss	35.8	(1.1)*	16.8	(3.7)	-5.1	(1.3)	-25.8	(2.4)*
Rear Boss	53.8	(3.3)*	30.7	(6.0)*	7.1	(5.3)	-7.4	(4.4)
Rear	16.3	(10.0)	1.3	(9.8)	-6.1	(4.7)	-30.9	(6.5)*

Error in Peak Rotational Velocity (rad/s)								
	13		**21**		**28**		**35**	
Front	-2.0	(0.4)	-1.7	(2.0)	-2.9	(1.2)	-3.4	(0.2)
Front Boss	3.9	(0.7)	2.8	(0.6)	-0.7	(1.2)	-3.4	(3.3)
Rear Boss	-1.7	(0.3)	-2.9	(0.2)	-4.3	(0.2)*	-4.2	(0.3)*
Rear	-3.8	(3.3)	-3.9	(0.5)	-10.9	(9.2)*	-10.9	(0.5)*

Error in Peak Rotational Acceleration (rad/s/s)								
	1746		**3288**		**4372**		**5853**	
Front	434.8	(384.4)	1602.4	(1127.5)*	-38.3	(658.1)	510.1	(785.0)
Front Boss	2858.3	(354.3)*	1909.4	(556.2)*	-593.7	(565.9)	-2254.9	(343.6)*
Rear Boss	4410.8	(300.6)*	3374.1	(363.8)*	3187.7	(519.9)*	1852.3	(850.4)*
Rear	885.7	(1129.0)	610.7	(466.3)	1430.7	(1966.5)*	-843.4	(223.2)

Consistent with the sensor error results, linear regression showed the lowest error occurring in rotational velocity (Table 21, Figure 10). Linear and rotational acceleration displayed low correlation for all locations. Peak linear acceleration given by Triax had large variability in the front and rear locations, and did not largely change with increasing impact magnitude in front boss and rear boss locations. Large variability was also seen in rotational acceleration. Although there was large variability, overall systematic error remained low for linear acceleration and rotational velocity with slopes remaining within 6% and 15% of 1.0 (Table 22). Rotational acceleration still had large systematic errors with an overall slope of 0.72.

Table 21: R^2 values from linear regressions constrained through the origin for helmeted Triax. LA, RV, and RA signify linear acceleration, rotational velocity, and rotational acceleration, respectively.

	LA	**RV**	**RA**
Front	-0.01	0.98	0.21
Front Boss	0.29	0.76	-0.15
Rear Boss	0.18	1.00	0.45
Rear	0.66	0.64	0.37
Total	0.15	0.79	0.19

Table 22: Slopes from linear regressions constrained through the origin for helmeted Triax. LA, RV, and RA signify linear acceleration, rotational velocity, and rotational acceleration, respectively.

	LA	RV	RA
Front	1.12	1.12	0.76
Front Boss	0.94	0.99	0.89
Rear Boss	0.75	1.15	0.58
Rear	1.13	1.30	0.86
Total	0.94	1.15	0.72

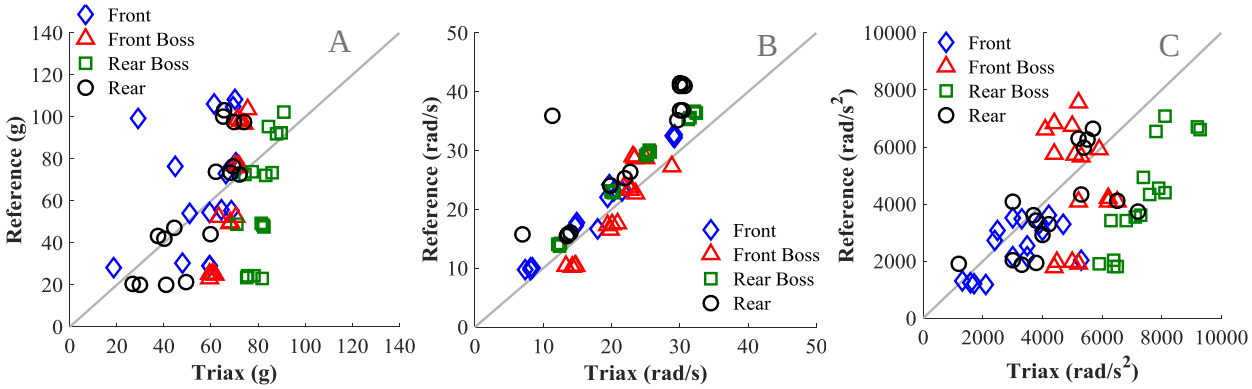

Figure 10: Peak reference values versus peak helmeted Triax values in linear acceleration (A), rotational velocity (B), and rotational acceleration (C). A 1:1 diagonal is drawn on each graph to visually show the amount of overprediction (points below line) and underprediction (points above line) of the reference.

The results from planned contrasts indicated significant differences in location and impact energies for all three kinematic variables ($p<0.05$).

Average NRMSE ranged from 12.4% to 53.8% in linear acceleration, 11.1% to 22.0% in rotational velocity, and 13.9% to 69.6% in rotational acceleration (Table 23). Triax displayed moderately similar shapes to the reference, although there were wide corridors in the sensor results indicating large variability for all kinematic variables (Figure A-11, Figure A-12, Figure A-13).

Table 23: Average (SD) NRMSE for helmeted Triax tests. Significance was concluded for almost every test condition for all three kinematic variables. The one exception was in rotational acceleration at the front boss, 75 g impact. Column headings in peak linear acceleration represent the targeted values, while column headings for the other variables are peak reference averages for each impact energy.

NRMSE in Peak Linear Acceleration (%)								
	25		**50**		**75**		**100**	
Front	30.7	(8.0)*	24.4	(4.5)*	22.6	(1.9)*	18.9	(5.0)*
Front Boss	35.2	(2.7)*	20.1	(1.7)*	12.6	(1.6)*	12.4	(4.5)*
Rear Boss	53.8	(3.9)*	22.9	(4.0)*	18.3	(2.2)*	15.1	(2.2)*
Rear	36.6	(9.6)*	22.1	(1.1)*	15.0	(4.6)*	21.5	(1.6)*

NRMSE in Peak Rotational Velocity (%)								
	12		**22**		**31**		**37**	
Front	14.8	(2.3)*	17.8	(0.6)*	13.8	(3.8)*	11.2	(1.2)*
Front Boss	15.1	(0.9)*	11.1	(0.6)*	11.1	(0.9)*	15.2	(2.0)*
Rear Boss	16.5	(1.0)*	12.1	(0.9)*	11.9	(0.6)*	13.1	(1.6)*
Rear	20.0	(10.2)*	13.3	(1.3)*	21.9	(17.9)*	14.4	(0.2)*

NRMSE in Peak Rotational Acceleration (%)								
	1377		**2538**		**3686**		**4824**	
Front	28.5	(11.6)*	38.3	(17.5)*	22.3	(3.3)*	19.5	(2.9)*
Front Boss	48.7	(2.2)*	28.0	(2.5)*	16.8	(1.2)	16.3	(4.6)*
Rear Boss	69.6	(9.9)*	38.5	(3.1)*	30.0	(2.2)*	23.5	(1.5)*
Rear	35.7	(5.3)*	25.8	(4.6)*	30.3	(10.3)*	13.9	(0.5)*

The results from planned contrasts indicated significant differences in location and impact energies for all three kinematic variables according to NRMSE ($p<0.05$).

GFT, GForce Tracker

Unhelmeted

GFT recorded all 64 impacts in the unhelmeted condition. Systematic error increased with impact energy in the front and front boss locations in linear acceleration. The rear boss and rear locations decreasing in systematic error with energy and had high random error throughout. In rotational velocity, sensor errors remained relatively constant with impact energy, although the front and front boss locations exhibited much lower systematic error than the rear boss and rear locations. The latter two locations also largely over-estimated the reference both in linear acceleration and rotational velocity.

Table 24: Average (SD) sensor error for unhelmeted GFT tests. Front boss, rear boss, and rear locations in linear acceleration exhibited significance from zero at various impact energies, as denoted by asterisks. Front, rear boss, and rear locations in rotational velocity exhibited significance in almost all impact energies. Column headings in peak linear acceleration represent the targeted values, while column headings for rotational velocity are peak reference averages for each impact energy.

	Peak Linear Acceleration (g)							
	25		**50**		**75**		**100**	
Front	1.5	(1.2)	1.1	(1.0)	-3.9	(1.0)	-20.1	(0.8)
Front Boss	-9.0	(2.1)	-19.9	(2.4)	-23.6	(12.0)*	-29.2	(10.5)*
Rear Boss	65.8	(15.9)*	21.7	(36.6)*	28.1	(25.1)*	15.3	(33.9)
Rear	59.8	(23.9)*	68.5	(4.2)*	17.4	(21.8)	39.2	(28.1)*

	Peak Rotational Velocity (rad/s)							
	13		**22**		**30**		**36**	
Front	-0.6	(3.8)	8.7	(1.3)*	10.9	(0.3)*	4.8	(2.2)*
Front Boss	-0.6	(0.9)	1.0	(1.2)	3.6	(2.2)	1.8	(7.5)
Rear Boss	19.7	(6.0)*	17.3	(0.9)*	21.8	(2.8)*	16.4	(5.0)*
Rear	27.1	(0.4)*	19.7	(1.9)*	23.0	(4.0)*	19.4	(1.4)*

According to the linear regressions, neither linear acceleration nor rotational velocity showed good overall correlation (Table 25, Figure 11). Similar to trends seen in sensor error, the front and front boss locations showed the best correlation for both kinematic variables, with R^2 above 0.83. Rear and rear boss locations both had large variations. Overall slopes showed systematic error for both kinematic variables: 0.73 and 0.65 for linear acceleration and rotational velocity (Table 26).

Table 25: R^2 values from linear regressions constrained through the origin for unhelmeted GFT. LA and RV signify linear acceleration and rotational velocity, respectively.

	LA	**RV**
Front	0.93	0.87
Front Boss	0.84	0.87
Rear Boss	-0.05	0.72
Rear	0.14	0.59
Total	-0.24	0.42

Table 26: Slopes from linear regressions constrained through the origin for unhelmeted GFT. LA and RV signify linear acceleration and rotational velocity, respectively.

	LA	**RV**
Front	1.12	0.78
Front Boss	1.44	0.92
Rear Boss	0.63	0.59
Rear	0.57	0.55
Total	0.73	0.65

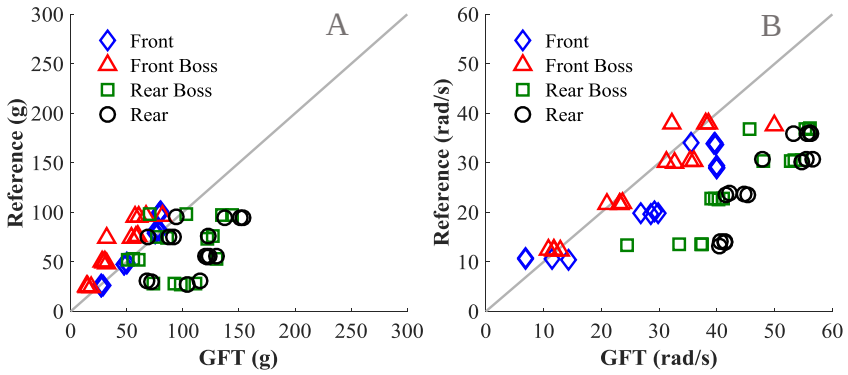

Figure 11: Peak reference values versus peak unhelmeted GFT values in linear acceleration (A) and rotational velocity (B). A 1:1 diagonal is drawn on each graph to visually show the amount of overprediction (points below line) and underprediction (points above line) of the reference.

The results from planned contrasts indicated significant differences in location and impact energy for both linear acceleration and rotational velocity ($p<0.05$).

For unhelmeted tests, average NRMSE ranged from 5.5% to 58.8% in linear acceleration and 6.6% to 99.0% in rotational velocity (Table 27). From a qualitative comparison of curves, GFT displayed similarity to reference for only the front location in linear acceleration (Figure A-14). In the remaining locations, the sensor underpredicted the reference peak. In rear boss and rear locations, a second large, shorter duration peak occurred around 20 ms. Rotational velocity curves did not display similarity to the reference and had large variations between tests as exhibited by wide corridors (Figure A-15).

Table 27: Average (SD) NRMSE for unhelmeted GFT tests. Significance, denoted by asterisks, was concluded for almost every test conditions for all three kinematic variables. Exceptions included the 50 g and 75 g impacts to the front in linear acceleration and the highest magnitude impact to the front in rotational velocity. Column headings in peak linear acceleration represent the targeted values, while column headings for rotational velocity are peak reference averages for each impact energy.

	NRMSE in Peak Linear Acceleration (%)							
	25		**50**		**75**		**100**	
Front	8.5	(1.6)*	6.4	(0.5)	5.5	(0.3)	8.5	(0.8)*
Front Boss	21.0	(1.1)*	20.9	(0.2)*	24.1	(2.4)*	20.6	(1.8)*
Rear Boss	58.8	(9.9)*	21.8	(14.0)*	15.6	(2.7)*	18.5	(2.6)*
Rear	56.7	(6.1)*	45.1	(1.1)*	28.3	(2.9)*	23.0	(2.8)*

	NRMSE in Peak Rotational Velocity (%)							
	13		**22**		**30**		**36**	
Front	31.6	(9.6)*	30.1	(1.4)*	23.4	(0.1)*	6.6	(1.5)
Front Boss	13.4	(4.5)*	16.3	(1.4)*	17.2	(2.6)*	13.8	(2.4)*
Rear Boss	52.9	(13.6)*	28.0	(12.6)*	37.2	(12.8)*	35.1	(3.8)*
Rear	99.0	(4.6)*	47.0	(6.4)*	25.1	(5.1)*	15.4	(1.4)*

The results from planned contrasts indicated significant differences in location and impact energies for both kinematic variables according to NRMSE ($p<0.05$).

Helmeted

GFT successfully recorded all 64 helmeted tests. Unlike the unhelmeted tests, helmeted GFT tests had increasing systematic error with impact energy at all locations for linear acceleration. Linear acceleration also consistently overpredicted the reference, especially at the rear boss and rear locations. Systematic error was largely constant in rotational velocity except for the highest impacts to the rear location (Table 28).

Table 28: Average (SD) sensor error for helmeted GFT tests. Significance, denoted by asterisks, in linear acceleration was found in almost all test conditions except for impacts at the 25 g energy level to the front and front boss. The only significance in rotational velocity occurred at the higher impact energies for the rear location. Column headings in peak linear acceleration represent the targeted values, while column headings for the other variables are peak reference averages for each impact energy.

	Peak Linear Acceleration (g)							
	25		**50**		**75**		**100**	
Front	11.4	(1.0)	35.2	(1.3)*	64.2	(8.5)*	74.1	(10.3)*
Front Boss	18.7	(1.6)	36.7	(10.5)*	64.1	(5.2)*	78.3	(11.8)*
Rear Boss	77.5	(2.4)*	109.1	(7.4)*	134.2	(5.7)*	137.8	(6.5)*
Rear	113.7	(2.5)*	151.6	(11.9)*	198.9	(2.8)*	191.7	(5.0)*

	Peak Rotational Velocity (rad/s)							
	13		**21**		**28**		**35**	
Front	0.9	(0.3)	-0.1	(0.6)	-1.5	(0.8)	-2.5	(1.0)
Front Boss	1.6	(0.3)	1.6	(0.7)	1.5	(2.5)	-0.9	(4.4)
Rear Boss	0.4	(0.2)	-0.9	(0.5)	-1.8	(0.8)	2.4	(1.3)
Rear	-0.9	(0.2)	-3.0	(0.7)	-5.4	(1.5)*	-9.2	(0.6)*

Regression results for the helmeted GFT tests showed that rotational velocity showed fairly good correlation to reference: individual location R^2 values remained above 0.87, and the overall value was 0.89 (Table 29, Figure 12). Linear acceleration locations individually had high R^2 values, although the overall R^2 was 0.39. Overall slopes showed large systematic error in linear acceleration, but low error in rotational velocity (Table 30). Slopes were 62% and 6% from 1.0, respectively.

Table 29: R^2 values from linear regressions constrained through the origin for helmeted GFT. LA and RV signify linear acceleration and rotational velocity, respectively.

	LA	RV
Front	0.96	0.98
Front Boss	0.97	0.86
Rear Boss	0.87	0.95
Rear	0.79	0.95
Total	0.39	0.89

Table 30: Slopes from linear regressions constrained through the origin for helmeted GFT. LA and RV signify linear acceleration and rotational velocity, respectively.

	LA	RV
Front	0.58	1.06
Front Boss	0.56	0.96
Rear Boss	0.36	0.99
Rear	0.28	1.20
Total	0.38	1.06

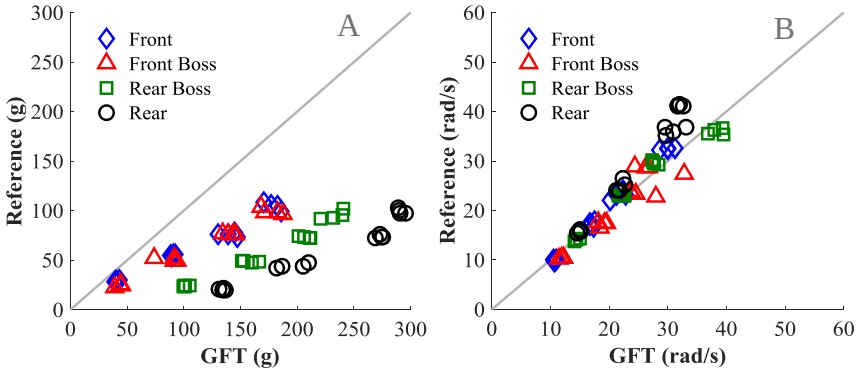

Figure 12: Peak reference values versus peak helmeted GFT values in linear acceleration (A) and rotational velocity (B). A 1:1 diagonal is drawn on each graph to visually show the amount of overprediction (points below line) and underprediction (points above line) of the reference.

The results from planned contrasts indicated significant differences in location and impact energy for both linear acceleration and rotational velocity ($p<0.05$).

For helmeted tests, average NRMSE ranged from 20.9% to 118.2% in linear acceleration and 5.4% to 21.4% in rotational velocity (Table 31). Qualitative comparisons of curve shapes in linear acceleration showed large overpredictions of the reference, especially in the rear boss and rear

locations (Figure A-16). Also, sensor peaks did not display similar shapes to the reference in these locations, with GFT experiencing a shorter-duration peak or double peak. Rotational velocity curves demonstrated better peak alignment, although the curves were not very similar between sensor and reference (Figure A-17).

Table 31: Average (SD) NRMSE for helmeted GFT tests. Significance was concluded for almost every test conditions for all three kinematic variables. The only exceptions occurred in rotational velocity at the lowest and highest impact energy for the front location. Column headings in peak linear acceleration represent the targeted values, while column headings for the other variables are peak reference averages for each impact energy.

	NRMSE in Peak Linear Acceleration (%)							
	25		**50**		**75**		**100**	
Front	31.2	(2.0)*	34.7	(1.1)*	31.7	(1.1)*	24.1	(2.6)*
Front Boss	33.8	(1.2)*	26.0	(6.1)*	23.9	(1.2)*	20.9	(2.1)*
Rear Boss	78.0	(1.4)*	48.7	(3.1)*	37.6	(2.4)*	29.0	(0.3)*
Rear	118.2	(5.3)*	82.1	(3.9)*	66.3	(1.6)*	48.2	(3.0)*

	NRMSE in Peak Rotational Velocity (%)							
	13		**21**		**28**		**35**	
Front	5.4	(0.3)	21.4	(1.1)*	19.5	(3.4)*	6.8	(1.3)
Front Boss	12.9	(1.0)*	11.9	(1.3)*	13.5	(0.4)*	18.5	(1.4)*
Rear Boss	9.1	(0.4)*	11.0	(0.3)*	13.0	(1.2)*	15.0	(1.9)*
Rear	15.6	(2.0)*	13.8	(2.7)*	13.1	(1.4)*	15.4	(0.3)*

The results from planned contrasts indicated significant differences in location and impact energy for linear acceleration, and significance in only impact energy for rotational velocity according to NRMSE ($p<0.05$).

Shockbox, i1 Biometrics (Impakt Protective)

Shockbox failed to record 9 of the 64 impacts, all at the 25 g impact energy level, despite having a linear acceleration threshold of 15 g. Shockbox was excluded from statistical analyses due to the low number of data points.

Table 32: Number of missed impacts by Shockbox at each test condition. These impacts all occurred at the lowest impact energy.

	25g	**50g**	**75g**	**100g**
Front	4	0	0	0
Front Boss	1	0	0	0
Rear Boss	4	0	0	0
Rear	0	0	0	0

Front, front boss, and rear boss locations consistently underpredicted the reference. Systematic error also increased with impact energy at all locations. Random error increased with impact energy for the rear boss location (Table 33).

Table 33: Average (SD) sensor error for helmeted Shockbox tests. Shockbox was excluded from statistical analysis due to the low number of data points. Column headings in peak linear acceleration represent the targeted values.

	Peak Linear Acceleration (g)							
	25		**50**		**75**		**100**	
Front			-34.5	(5.1)	-44.1	(17.8)	-82.5	(5.5)
Front Boss	-12.6	(3.2)	-33.6	(1.3)	-57.0	(2.4)	-76.2	(1.8)
Rear Boss			-32.6	(7.3)	-49.9	(5.8)	-49.1	(20.7)
Rear	8.3	(4.7)	-18.5	(12.7)	3.2	(6.8)	-22.8	(5.8)

Shockbox correlated fairly well with the reference in front boss and rear locations with R^2 of 0.71 and 0.73 (Table 34, Figure 13). However, there was not even positive correlation for the front and rear boss locations. Slopes for each location ranged from 11% to over 100% from 1.0, with the overall slope being 1.6 (Table 35).

Table 34: R^2 values from linear regressions constrained through the origin for helmeted Shockbox. LA signifies linear acceleration, rotational velocity, and rotational acceleration, respectively.

	LA
Front	-2.22
Front Boss	0.70
Rear Boss	-1.40
Rear	0.73
Total	-1.19

Table 35: Slopes from linear regressions constrained through the origin for helmeted Shockbox. LA signifies linear acceleration, rotational velocity, and rotational acceleration, respectively.

	LA
Front	2.67
Front Boss	3.68
Rear Boss	2.03
Rear	1.11
Total	1.60

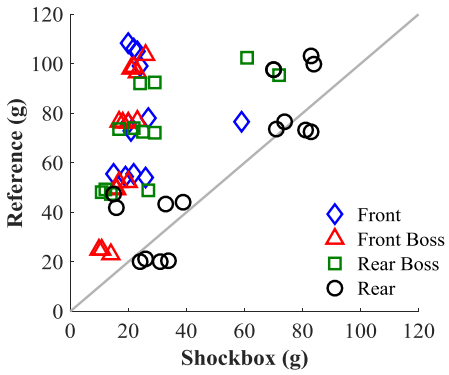

Figure 13: Peak reference values versus peak helmeted Shockbox values in linear acceleration. A 1:1 diagonal is drawn on each graph to visually show the amount of overprediction (points below line) and underprediction (points above line) of the reference.

Shockbox does not output time series data for each impact, so NRMSE could not be calculated.

HeadsUp, Integrated Bionics

HeadsUp failed to record 16 of the 64 impacts (Table 36). Most of these impacts occurred at the lower magnitudes, despite the sensor having a threshold of HIC = 10. The only location in which missed impacts are understandable is the front boss location which resulted in HIC values of 11-13 in the lowest energy impacts. The remaining locations had HIC values over 15. HeadsUp was excluded from statistical analyses due to the low number of data points.

Table 36: Number of missed impacts by HeadsUp at each test condition. The majority higher magnitude impacts were recorded, but many of the lowest magnitude impacts were missed.

	25g	50g	75g	100g
Front	4	2	1	0
Front Boss	4	4	1	1
Rear Boss	2	1	0	0
Rear	1	1	0	0

Most test conditions overpredicted the reference. Systematic and random error increased with impact energy for all but the front boss location (Table 37).

Table 37: Average (SD) sensor error for helmeted HeadsUp tests. HeadsUp was excluded from statistical analysis due to the low number of data points. Column headings in peak linear acceleration represent the targeted values.

	Peak Linear Acceleration (g)							
	25		50		75		100	
Front			76.1	(19.0)	-30.7	(22.5)	-15.1	(40.1)
Front Boss					17.0	(26.4)	-34.2	(3.7)
Rear Boss	8.3	(5.6)	11.8	(3.2)	90.2	(58.1)	119.8	(22.7)
Rear	23.2	(14.9)	28.4	(20.2)	73.2	(37.4)	86.5	(27.7)

The rear location showed highest correlation to reference with R^2 equal to 0.77 (Table 38, Figure 14). However, correlations for the remaining locations were low or even negative. Slopes for each location ranged from 11% to over 100% from 1.0, with the overall slope being 1.6 (Table 35).

Table 38: R^2 values from linear regressions constrained through the origin for helmeted HeadsUp. LA signifies linear acceleration, rotational velocity, and rotational acceleration, respectively.

	LA
Front	-3.77
Front Boss	-3.50
Rear Boss	0.56
Rear	0.77
Total	-0.73

Table 39: Slopes from linear regressions constrained through the origin for helmeted HeadsUp. LA signifies linear acceleration, rotational velocity, and rotational acceleration, respectively.

	LA
Front	0.80
Front Boss	1.02
Rear Boss	0.45
Rear	0.51
Total	0.54

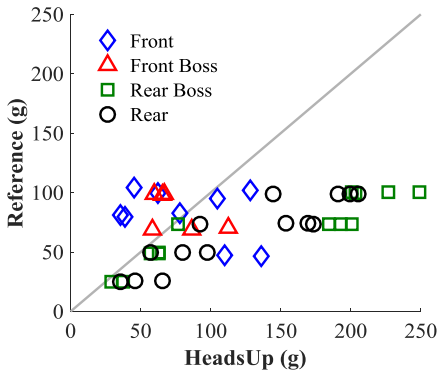

Figure 14: Peak reference values versus peak helmeted HeadsUp values in linear acceleration. A 1:1 diagonal is drawn on each graph to visually show the amount of overprediction (points below line) and underprediction (points above line) of the reference.

HeadsUp does not output time series data for each impact, so NRMSE could not be calculated.

DISCUSSION

The laboratory methods developed within this thesis make up Phase I of a two-phased approach to evaluate wearable sensors. Through laboratory testing, sensors were evaluated in an ideal scenario that does not take into account additional factors such as variations in sensor placement, sweat, hair, skin movement, and false hits. Phase II consists of on-field tests and cadaver tests that will better evaluate each sensor under the conditions listed. On-field tests include all possible factors that could cause the sensors to collect erroneous data, although there is currently no available reference accelerometer or gyroscope to ensure validity in kinematic output of the wearable sensors. Instead, on-field tests will be used to test the number of false positives (untrue impacts falsely recorded by the sensor) as well as false negatives (true impacts not recorded by the sensor) during actual use by consumers in sports practices and games. Phase II will be implemented by instrumenting adult male or female athletes with a sensor during several days of regular practice or games in any sport for which the sensor is recommended for use. Sensor impact counts will be compared to video data taken during the time of sensor use to verify true and false impacts. Youth athletes will not be instrumented since head circumference is already over 90% full-grown by age six, correlating to a 0.6 – 0.8 cm difference in head radius between children and adults.[42] In transforming the linear acceleration to the center of gravity of the headform, this minor difference in radius corresponds to less than a 3% error in peak acceleration. Cadaver tests will be utilized to identify the effects of factors that cannot be easily replicated on a headform, such as skin movement and hair, by comparing sensor output to reference. Cadaver tests provide a much more realistic scenario than headform impacts, although they are very expensive and labor intensive. As a result, the headform tests in Phase I provide an easier, faster, less expensive first analysis of each sensor. Those that perform well under the ideal conditions will be evaluated in Phase II. The results from this two-phased approach form the basis for an overall Sensor STAR evaluation.

REFERENCE REPEATABILITY

Overall, the reference sensors used in this analysis displayed excellent to acceptable repeatability within most test conditions. Higher variability was seen in the 25 g impacts in linear acceleration because the test constraint of ±5 g inherently resulted in greater percent error from the mean compared to the higher magnitude impacts. Marginal to poor repeatability was also observed in the rotational acceleration conditions, especially the helmeted rear tests. These results are not

surprising since rotational acceleration is not measured directly by the reference sensors, but instead is calculated from the rotational velocity. Rotational velocity COV is highest for the helmeted rear location, and these results are compounded when differentiated to find rotational acceleration. For all conditions, however, lower variability exists if COV is calculated for each sensor instead of across all tests.

Although there was marginal to poor repeatability in some conditions, this only affects statistical comparisons between sensors or test conditions. Since the major results of this thesis are based on differences between reference and wearable sensors and not repeatability of the wearable sensors themselves, variability in reference values does not play a large role.

OVERALL SENSOR ASSESSMENT AND IMPLICATIONS

The HIT System has been well-validated in the laboratory under various conditions.[43-46] As a whole, R^2 correlations to reference in linear acceleration are above 0.9, with a slope of 1.0.[43] However, different test conditions can provide different results.[46] To account for variability in test setups, acceptable error for Phase I was set to be an overall R^2 of 0.80 and slope between 0.80 and 1.20 from the linear regression constrained through the origin. These conditions must be fulfilled in at least one kinematic variable for the sensor to be further evaluated in Phase II.

xPatch, X2 Biosystems

Unhelmeted

Unhelmeted X2 displayed high overall R^2 values and slopes near 1.0 for both linear acceleration and rotational velocity, well within the conditions for Phase II. However, rotational acceleration exhibited an overall R^2 of 0.61 and slope of 1.65. However, individual location correlations remained above 0.93 and random errors were low, indicating it may be possible to correct for the location differences in post-processing. These results indicate that unhelmeted X2 contains adequately low error in linear acceleration and rotational velocity to continue with Phase II on-field and cadaver tests. However, caution must be taken when examining rotational acceleration, as additional correction factors may be needed to obtain more accurate measurements.

Helmeted

Helmeted X2 gave slightly higher errors in linear acceleration, although values still fell within the acceptable range for Phase II tests. Random errors in most test conditions remained below 3 g except in the rear boss and rear locations. At those two locations, spikes occurred in the time series, almost indistinguishable from the true peak. Their cause may have been some form of helmet interaction with the sensor, since the rear boss and rear locations are in close proximity to the sensor placement behind the ear. Although these spikes were not large enough to decrease overall error in the sensor, they did affect the random error since they were not observed in every test of the same condition. Despite these instances, the overall R^2 was 0.86. Rotational velocity performed much more accurately, with an overall R^2 of 0.95 and slope of 0.99. The only discrepancy was the test condition with the erroneous first data point. By identifying the true peak with the time series data rather than peak output, this problem can be eliminated. Rotational acceleration performed poorly, with an overall R^2 of 0.13 and slope of 1.41. Similar to the unhelmeted condition, this error may be corrected for in post-processing since random errors are relatively small for each location. These results indicate that helmeted X2 contains adequately low error in linear acceleration and rotational velocity to continue with Phase II on-field and cadaver tests. However, obtaining peak values from time series data rather than automatic outputs would give more reliable results, especially in rotational velocity. Also, caution must be taken when examining rotational acceleration, as additional correction factors may be needed to obtain more accurate measurements.

Vector Mouth Guard, i1 Biometrics

Vector MG exhibited significant location differences in linear acceleration. The large limitation in testing that could have attributed to this was the inability to test the mouth guard in a realistic manner. Instead of firmly fixed to the headform, the mouth guard was adhered with multiple layers of adhesives. Although this fastening method seemed adequate, high-speed video may identify movement in the sensor with respect to the headform at some locations. Irrespective of the location differences, individual R^2 values remained above 0.96. However, the overall R^2 was 0.70 and the slope was 0.80. Additional test methods or correction factors could be implemented to decrease the systematic error component since individual random error was low. Rotational velocity offered

excellent accuracy compared to the other variables. The R^2 value remained above 1.00 and the slope was 1.04. Rotational acceleration exhibited significant location differences, similar to linear acceleration. Although individual R^2 values fell above 0.99, the overall correlation was 0.73 and slope was 1.47. This location-dependent error can possibly be corrected for in post-processing. These results indicate that Vector MG may contain adequate error in linear acceleration after different test conditions are developed or correction factors are implemented. Rotational velocity contains adequately low error to continue with Phase II on-field and cadaver tests, however most consumers and researchers focus more on linear acceleration measurements than rotational velocity. Caution must be taken when examining rotational acceleration, as additional correction factors may be needed to obtain more accurate measurements.

SIM-G, Triax Technologies

Unhelmeted

Unhelmeted Triax tests contained significant differences in location and wide variability in systematic and random error among test conditions. In linear acceleration, Triax peak values did not exceed 86 g; therefore all 100 g tests exhibited large systematic error. Many test conditions also included up to 17 g in random error. With random error so high in some conditions, accuracy will not be greatly increased with simple correction factors. Impacts to the front and rear locations especially showed low correlations to reference with R^2 below 0.4. The overall slope of the regression was 1.06, within the requirements for Phase II tests, although the overall R^2 value was 0.25. Rotational velocity contained better accuracy: although significant differences in locations were present, the overall R^2 correlation still remained above 0.93 and the slope was 1.12, within the conditions for Phase II. Rotational acceleration tells a similar story to linear acceleration, with wide variations among test conditions. Although low random errors exist in some conditions, the overall R^2 value was -0.56 and slope was 0.46. At its current state, unhelmeted Triax contains large errors in linear and rotational acceleration that cannot be resolved with simple corrections. However, since the rotational velocity regression remained within the requirements for additional tests, unhelmeted Triax will continue with on-field and cadaver tests.

Helmeted

Similar to the unhelmeted tests, helmeted Triax results gave significant differences in location, wide variability in error among test conditions, and the peak values did not exceed 90 g. For the front boss and rear boss locations, impact magnitude did not largely change with impact energy, resulting in large error in the low-energy impacts and poor correlations to reference. The overall slope of the linear regression was 0.94, however the R^2 value was 0.15. Errors were significantly higher than those seen in the unhelmeted condition, indicating a possible physical effect of the helmet on the sensor. With a helmeted headform, the sensor stays in constant contact with the helmet. Consequently, the helmet may cause extra movement of the sensor at all impact locations. Rotational velocity contained lower error, although still did not fall within conditions for Phase II tests with a slope of 1.15 and R^2 of 0.79. Rotational acceleration exhibited large random errors in all test conditions and low correlations. With this combination, simple corrections cannot be performed. At its current state, unhelmeted Triax contains large errors in all kinematic variables and does not qualify for Phase II on-field and cadaver tests.

GFT, GForce Tracker

Unhelmeted

Unhelmeted GFT exhibited differences in location with the largest errors occurring in the rear boss and rear locations. Those two locations also had second peaks in the time series around the 20 ms mark. The peaks may have occurred due to poor coupling between the headband and headform. The GFT headband is a simple design with no added measures such as a rubber grip to ensure proper coupling to the headform. In the rear boss and rear locations, the resultant headform motion at impact is directed away from the sensor which is located at the back of the head. The headband could lag behind the impact, de-couple from the headform, and then spring back, experiencing a second impact against the headform. Actual movement of the headband must be confirmed with high-speed video. If this second peak was ignored and the true impact occurred before 20 ms, overall sensor error would be greatly reduced. Correlations for those locations would be 0.72 and 0.66 instead of currently below 0.1. Without the corrections, the overall R^2 value is -0.24 and slope is 0.73. Although some accuracy in linear acceleration can be resolved, no corrections can be performed to rotational velocity due to variable error and low individual correlations. Overall, the R2 correlation is 0.42 and slope is 0.65. At its current state, unhelmeted GFT contains large errors

in both kinematic variables that cannot be resolved with simple corrections. Even though more accuracy can be resolved in linear acceleration by obtaining peak values from time series data rather than automatic outputs, errors are still outside the acceptable conditions for Phase II on-field and cadaver tests.

Helmeted

Helmeted GFT exhibited an overall R^2 value of 0.39 and linear regression slope of 0.38 in linear acceleration. However, unlike the unhelmeted tests, there were low random errors for each test condition despite large overpredictions in systematic error. Therefore, it may be possible to apply correction factors to decrease the overall systematic error and obtain higher accuracy. Largest systematic errors occurred in the rear boss and rear locations. These large errors may be partly due to the fact that those two locations are closest to the sensor position on the inside shell of the helmet. Rotational velocity exhibited low error, with an R2 of 0.89 and slope of 1.06, well within the conditions for Phase II tests. Although helmeted GFT did not perform well in linear acceleration, rotational velocity results displayed adequately low error to continue to Phase II on-field and cadaver tests.

Shockbox, i1 Biometrics (Impakt Protective)

Shockbox was unreliable in recording all low-level head impacts. This is especially problematic because over 50% of all head impacts in football for youth, high school, and collegiate athletes occur below 20 g.[24,37,39,47,48] For the recorded impacts, most test conditions largely underpredicted the reference and experienced up to 20 g in random error. Correlations also were negative in the front and rear boss locations. As a result of all these error combinations, simple corrections could not be applied to increase overall accuracy. An overall linear regression gave an R^2 value of -1.19 and slope of 1.60. At its current state, Shockbox does not qualify for Phase II on-field and cadaver tests.

HeadsUp, Integrated Bionics

HeadsUp was unreliable in recording impacts at all energy levels, only recording 75% of total impacts. Correlations were negative in the front and front boss locations, with an overall R^2 correlation of -0.73. The slope of the linear regression was 0.54. As a result of large random error

within test conditions, simple corrections could not be applied to increase overall accuracy. At its current state, HeadsUp does not qualify for Phase II on-field and cadaver tests.

CONCLUSIONS

This study demonstrated that head impact sensor accuracy and reliability vary greatly between commercially available products, and highlights the need for objective and public data characterizing sensor quality. Although laboratory tests are an ideal scenario for evaluation and do not identify all possible factors associated with error, they offer as a good first estimate of sensor error. To allow for variation in test setups, an acceptable error threshold for Phase I was determined to be an R^2 value of 0.80 and slope between 0.80 and 1.20 for the linear regression constrained through the origin. These conditions must be fulfilled in at least one kinematic variable for the sensor to be further evaluated in Phase II. Unhelmeted and helmeted X2, Vector MG, unhelmeted Triax, and helmeted GFT all passed this threshold for at least one kinematic variable and will be further evaluated in Phase II on-field and cadaver tests. The remaining sensors will be retested under laboratory conditions after additional corrections are applied by the manufacturer to increase overall accuracy. It is important to note that these results do not provide a full analysis of these sensors, and caution should always be taken when interpreting results.

Wearable head impact sensors have many promising benefits for both consumers and researchers such as objectively identifying severe impacts and investigating head impact biomechanics in unhelmeted sports. However, they are currently not held to a standard of accuracy as displayed by large errors and low reliability even in ideal laboratory tests. By creating an objective evaluation of these sensors, consumers and researchers can be informed of their differences and manufacturers can be encouraged to create a product that will become a valuable tool to aid in the identification of head impacts in sports.

REFERENCES

1. Langlois JA, Rutland-Brown W, Wald MM. The epidemiology and impact of traumatic brain injury: a brief overview. *The Journal of head trauma rehabilitation.* 2006;21(5):375-378.
2. Gavett BE, Stern RA, McKee AC. Chronic traumatic encephalopathy: a potential late effect of sport-related concussive and subconcussive head trauma. *Clin Sports Med.* 2011;30(1):179-188, xi.
3. McKee AC, Cantu RC, Nowinski CJ, et al. Chronic Traumatic Encephalopathy in Athletes: Progressive Tauopathy following Repetitive Head Injury. *Journal of neuropathology and experimental neurology.* 2009;68(7):709-735.
4. Omalu BI, DeKosky ST, Minster RL, Kamboh MI, Hamilton RL, Wecht CH. Chronic traumatic encephalopathy in a National Football League player. *Neurosurgery.* 2005;57(1):128-134; discussion 128-134.
5. Covassin T, Elbin R, Sarmiento K. Educating coaches about concussion in sports: evaluation of the CDC's "Heads Up: Concussion in Youth Sports" initiative. *Journal of school health.* 2012;82(5):233-238.
6. McCrea M, Hammeke T, Olsen G, Leo P, Guskiewicz K. Unreported concussion in high school football players: implications for prevention. *Clin J Sport Med.* 2004;14(1):13-17.
7. Williamson IJ, Goodman D. Converging evidence for the under-reporting of concussions in youth ice hockey. *British journal of sports medicine.* 2006;40(2):128-132; discussion 128-132.
8. Register-Mihalik JK, Guskiewicz KM, McLeod T, Linnan LA, Mueller FO, Marshall SW. Knowledge, attitude, and concussion-reporting behaviors among high school athletes: a preliminary study. *Journal of athletic training.* 2012;48(5):645-653.
9. Langburt W, Cohen B, Akhthar N, O'Neill K, Lee JC. Incidence of concussion in high school football players of Ohio and Pennsylvania. *J Child Neurol.* 2001;16(2):83-85.
10. Povlishock JT. The window of risk in repeated head injury. *Journal of neurotrauma.* 2013;30(1):1-1.
11. Guskiewicz KM, McCrea M, Marshall SW, et al. Cumulative effects associated with recurrent concussion in collegiate football players: the NCAA Concussion Study. *Jama.* 2003;290(19):2549-2555.
12. LaBella C. A comparative analysis of injury rates and patterns among girls' soccer and basketball players at schools with and without athletic trainers from 2006/07-2008/09. Paper presented at: 2012 AAP National Conference and Exhibition2012.
13. Pryor RR, Casa DJ, Vandermark LW, et al. Athletic training services in public secondary schools: a benchmark study. *Journal of athletic training.* 2015;50(2):156-162.
14. *Report on Trends and Participation in Organized Youth Sports.* National Council of Youth Sports.
15. NCAA. Student-Athletes. http://www.ncaa.org/student-athletes. Accessed Nov. 30, 2015.
16. Daneshvar DH, Nowinski CJ, McKee AC, Cantu RC. The epidemiology of sport-related concussion. *Clin Sports Med.* 2011;30(1):1-17, vii.
17. Merkel DL, Molony Jr JT. Medical sports injuries in the youth athlete: emergency management. *International journal of sports physical therapy.* 2012;7(2):242.

18. Duma SM, Rowson S. Past, present, and future of head injury research. *Exerc Sport Sci Rev.* 2011;39(1):2-3.
19. Funk JR, Duma SM, Manoogian SJ, Rowson S. Development of Concussion Risk Curves Based on Head Impact Data from Collegiate Football Players. Paper presented at: Injury Biomechanics Research, Proceedings of the Thirty-Fourth Internation Workshop2006.
20. Funk JR, Rowson S, Daniel RW, Duma SM. Validation of Concussion Risk Curves for Collegiate Football Players Derived from HITS Data. *Ann Biomed Eng.* 2012;40(1):79-89.
21. Rowson S, Duma SM, Beckwith JG, et al. Rotational head kinematics in football impacts: an injury risk function for concussion. *Ann Biomed Eng.* 2012;40(1):1-13.
22. Rowson S, Duma SM. Development of the STAR Evaluation System for Football Helmets: Integrating Player Head Impact Exposure and Risk of Concussion. *Ann Biomed Eng.* 2011;39(8):2130-2140.
23. Rules Changes Regarding Practice & Concussion Prevention. 2012; http://www.popwarner.com/About_Us/Pop_Warner_News/Rule_Changes_Regarding_Practice___Concussion_Prevention_s1_p3977.htm. Accessed December 8, 2012.
24. Cobb BR, Urban JE, Davenport EM, et al. Head Impact Exposure in Youth Football: Elementary School Ages 9–12 Years and the Effect of Practice Structure. *Ann Biomed Eng.* 2013;41(12):2463-2473.
25. Pellman EJ, Powell JW, Viano DC, et al. Concussion in professional football: epidemiological features of game injuries and review of the literature--part 3. *Neurosurgery.* 2004;54(1):81-94; discussion 94-86.
26. NFL moves kickoffs to 35-yard line; touchbacks unchanged. 2011; http://www.nfl.com/news/story/09000d5d81ee38c1/article/nfl-moves-kickoffs-to-35yard-line-touchbacks-unchanged. Accessed November 2, 2015.
27. Hootman JM, Dick R, Agel J. Epidemiology of collegiate injuries for 15 sports: summary and recommendations for injury prevention initiatives. *Journal of athletic training.* 2007;42(2):311-319.
28. Marar M, McIlvain NM, Fields SK, Comstock RD. Epidemiology of concussions among United States high school athletes in 20 sports. *The American journal of sports medicine.* 2012;40(4):747-755.
29. Agel J, Olson DE, Dick R, Arendt EA, Marshall SW, Sikka RS. Descriptive epidemiology of collegiate women's basketball injuries: National Collegiate Athletic Association Injury Surveillance System, 1988-1989 through 2003-2004. *Journal of athletic training.* 2007;42(2):202-210.
30. Covassin T, Schatz P, Swanik CB. Sex differences in neuropsychological function and post-concussion symptoms of concussed collegiate athletes. *Neurosurgery.* 2007;61(2):345-351.
31. Campbell KR, Warnica MJ, Levine IC, et al. Laboratory Evaluation of the gForce Tracker™, a Head Impact Kinematic Measuring Device for Use in Football Helmets. *Annals of biomedical engineering.* 2015:1-11.
32. Higgins M, Halstead PD, Snyder-Mackler L, Barlow D. Measurement of impact acceleration: mouthpiece accelerometer versus helmet accelerometer. *Journal of athletic training.* 2007;42(1):5.
33. Nevins D, Smith L, Kensrud J. Laboratory Evaluation of Wireless Head Impact Sensor. *Procedia Engineering.* 2015;112:175-179.

34. Wong RH, Wong AK, Bailes JE. Frequency, magnitude, and distribution of head impacts in Pop Warner football: The cumulative burden. *Clinical Neurology and Neurosurgery.* 2014;118:1-4.
35. Wu LC, Nangia V, Bui K, et al. In vivo evaluation of wearable head impact sensors. *arXiv preprint arXiv:1503.03948.* 2015.
36. Wilcox BJ, Beckwith JG, Greenwald RM, et al. Head impact exposure in male and female collegiate ice hockey players. *Journal of biomechanics.* 2014;47(1):109-114.
37. Rowson S, Brolinson G, Goforth M, Dietter D, Duma SM. Linear and angular head acceleration measurements in collegiate football. *Journal of biomechanical engineering.* 2009;131(6):061016.
38. Cobb BR, Zadnik AM, Rowson S. Comparative analysis of helmeted impact response of Hybrid III and National Operating Committee on Standards for Athletic Equipment headforms. *Proceedings of the Institution of Mechanical Engineers, Part P: Journal of Sports Engineering and Technology.* 2015:1754337115599133.
39. Daniel RW, Rowson S, Duma SM. Head Impact Exposure in Youth Football. *Ann Biomed Eng.* 2012;40(4):976-981.
40. Pellman EJ, Viano DC, Tucker AM, Casson IR, Waeckerle JF. Concussion in professional football: reconstruction of game impacts and injuries. *Neurosurgery.* 2003;53(4):799-814.
41. Siegmund GP, Guskiewicz KM, Marshall SW, DeMarco AL, Bonin SJ. A headform for testing helmet and mouthguard sensors that measure head impact severity in football players. *Annals of biomedical engineering.* 2014;42(9):1834-1845.
42. Rollins JD, Collins JS, Holden KR. United States head circumference growth reference charts: birth to 21 years. *The Journal of pediatrics.* 2010;156(6):907-913. e902.
43. Beckwith JG, Greenwald RM, Chu JJ. Measuring Head Kinematics in Football: Correlation Between the Head Impact Telemetry System and Hybrid III Headform. *Ann Biomed Eng.* 2012;40(1):237-248.
44. Crisco JJ, Chu JJ, Greenwald RM. An algorithm for estimating acceleration magnitude and impact location using multiple nonorthogonal single-axis accelerometers. *Journal of biomechanical engineering.* 2004;126(6):849-854.
45. Chu JJ, Beckwith JG, Crisco JJ, Greenwald R. A Novel Algorithm to Measure Linear and Rotational Head Acceleration Using Single-Axis Accelerometers. *Journal of biomechanics.* 2006;39 supplement 1:S534.
46. Jadischke R, Viano DC, Dau N, King AI, McCarthy J. On the accuracy of the Head Impact Telemetry (HIT) System used in football helmets. *Journal of biomechanics.* 2013.
47. Broglio SP, Surma T, Ashton-Miller JA. High school and collegiate football athlete concussions: a biomechanical review. *Ann Biomed Eng.* 2012;40(1):37-46.
48. Daniel RW, Rowson S, Duma SM. Head Impact Exposure in Youth Football: Middle School Ages 12–14 Years. *Journal of biomechanical engineering.* 2014;136(9):094501.

APPENDIX: Time Series Averages

Averaged time series for sensor and reference for each test condition are shown graphically. Corridors represent ± 1 standard deviation at each time point. Sensor and reference curves were aligned by minimizing RMS error over the entire time series.

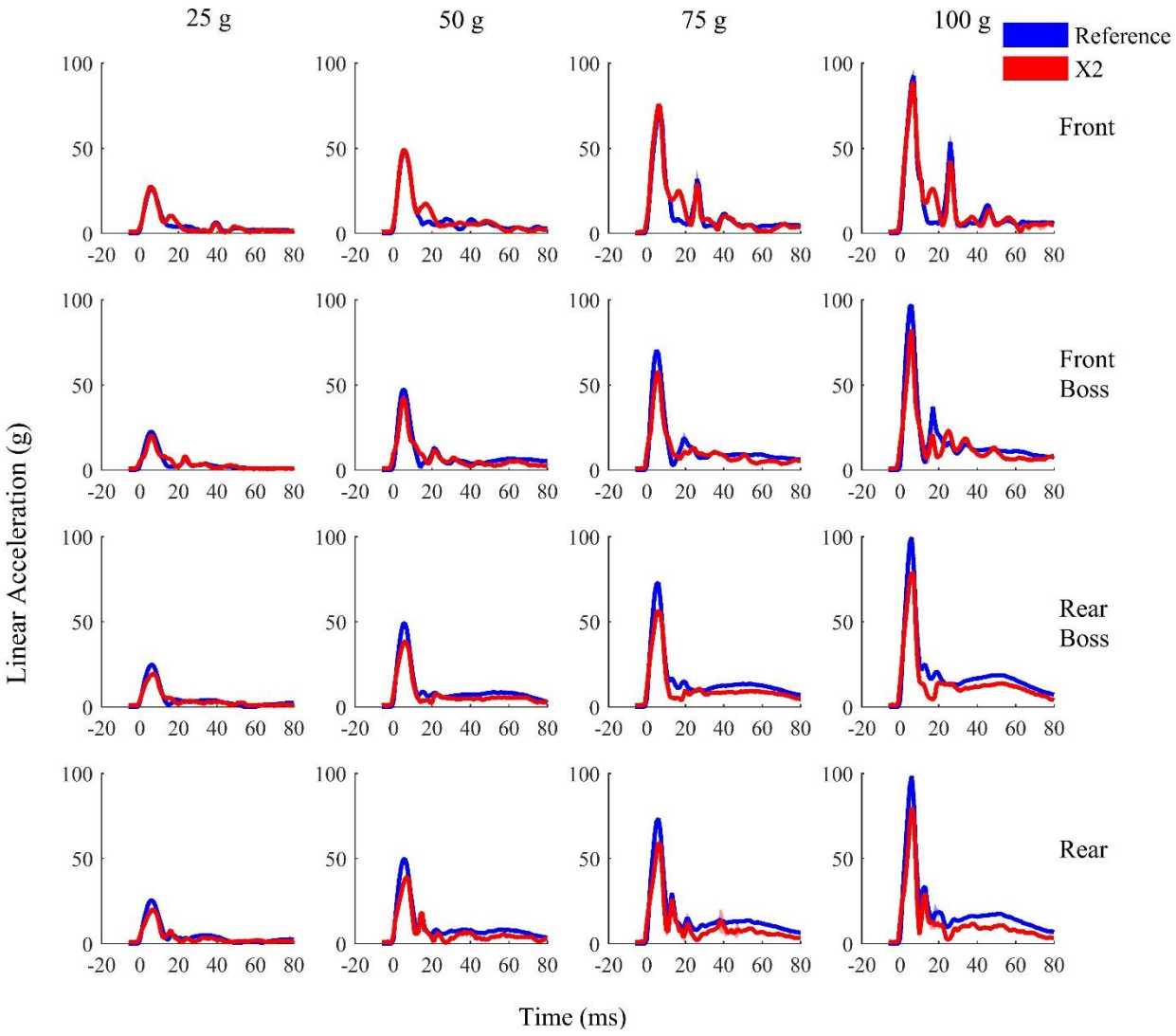

Figure A-1: Averaged unhelmeted X2 (red) and reference (blue) time series in linear acceleration. There were many similarities in curve shapes between X2 and reference.

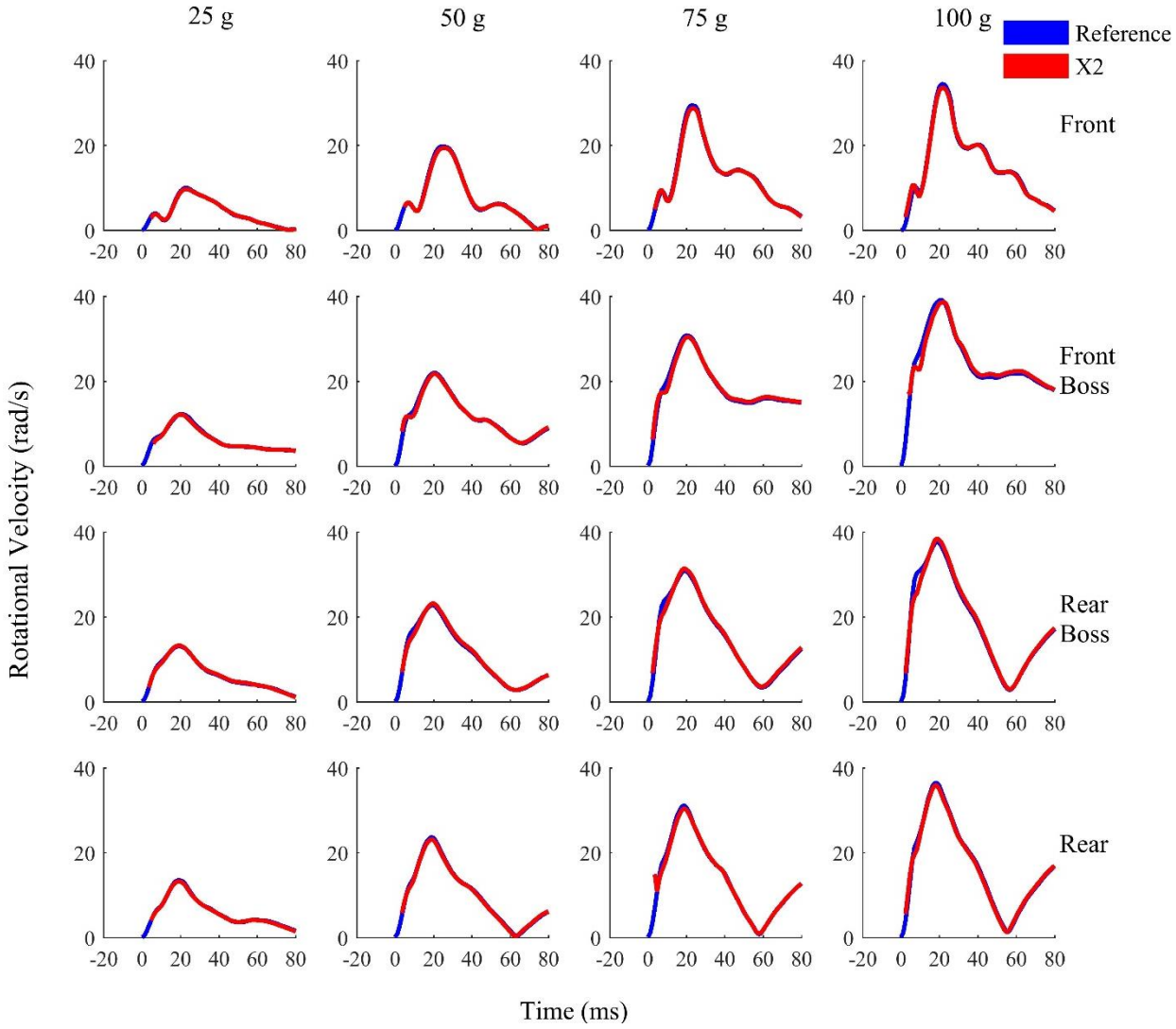

Figure A-2: Averaged unhelmeted X2 (red) and reference (blue) time series in rotational velocity. There were many similarities in curve shapes between X2 and reference.

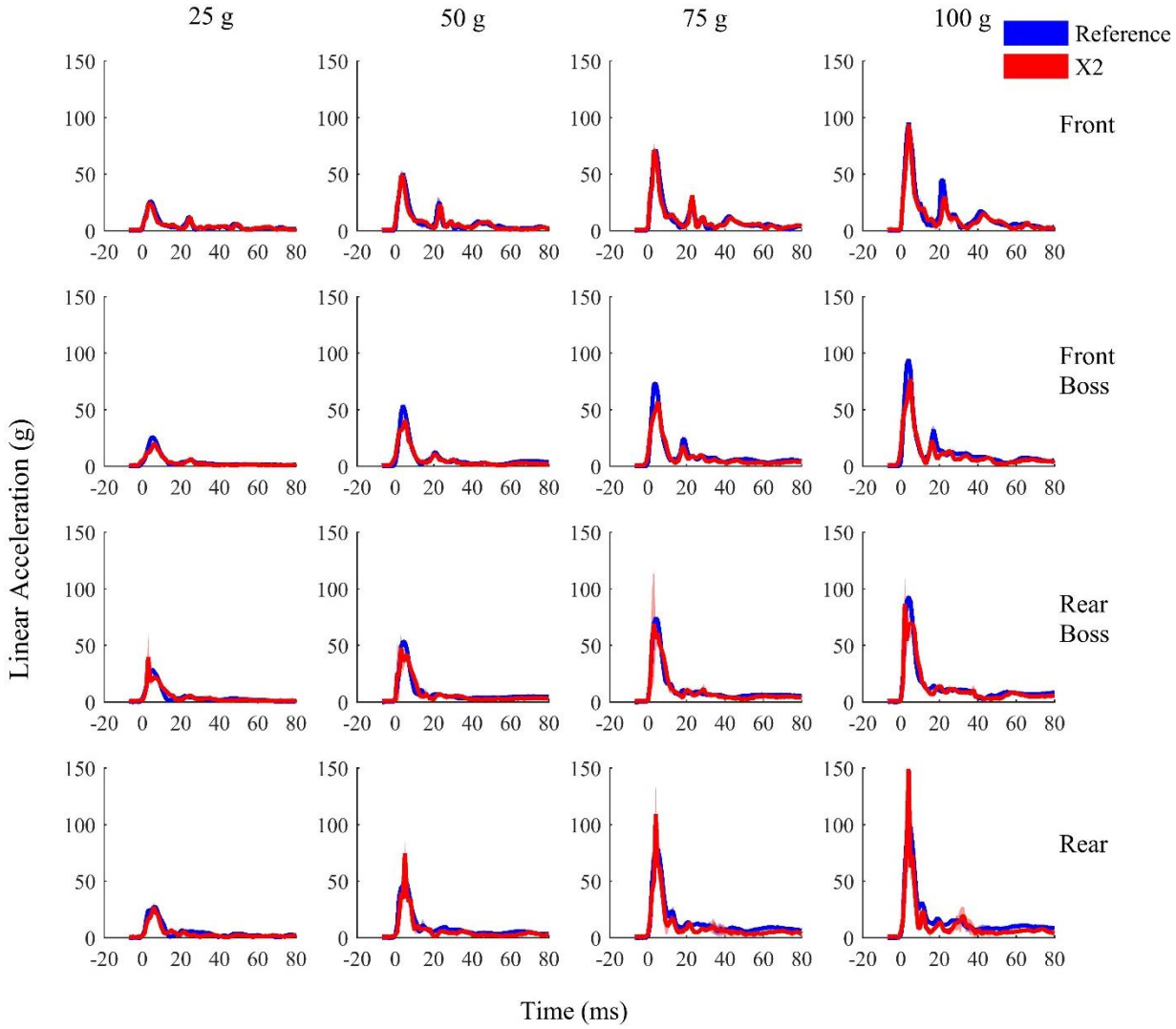

Figure A-3: Averaged helmeted X2 (red) and reference (blue) time series in linear acceleration. There were many similarities in curve shapes for the front and front boss locations, although spikes occurred in the sensor just before the peak in the rear boss and rear locations. These may have been due to the proximity of the impact to the sensor placement on the headform.

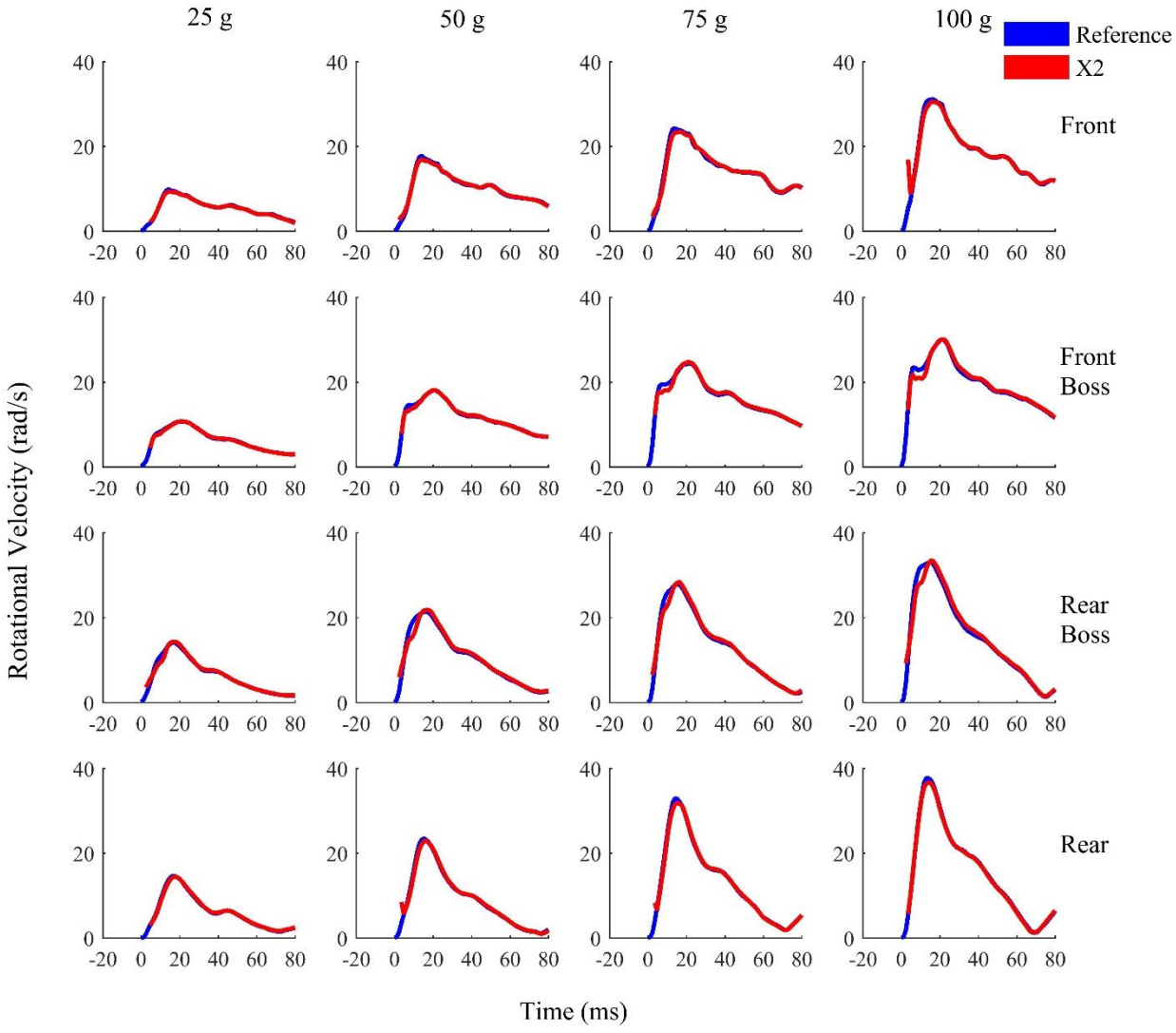

Figure A-4: Averaged helmeted X2 (red) and reference (blue) time series in rotational velocity. There were many similarities in curve shapes for all locations. Occasionally there was an erroneous first data point as seen in the front location at 100 g.

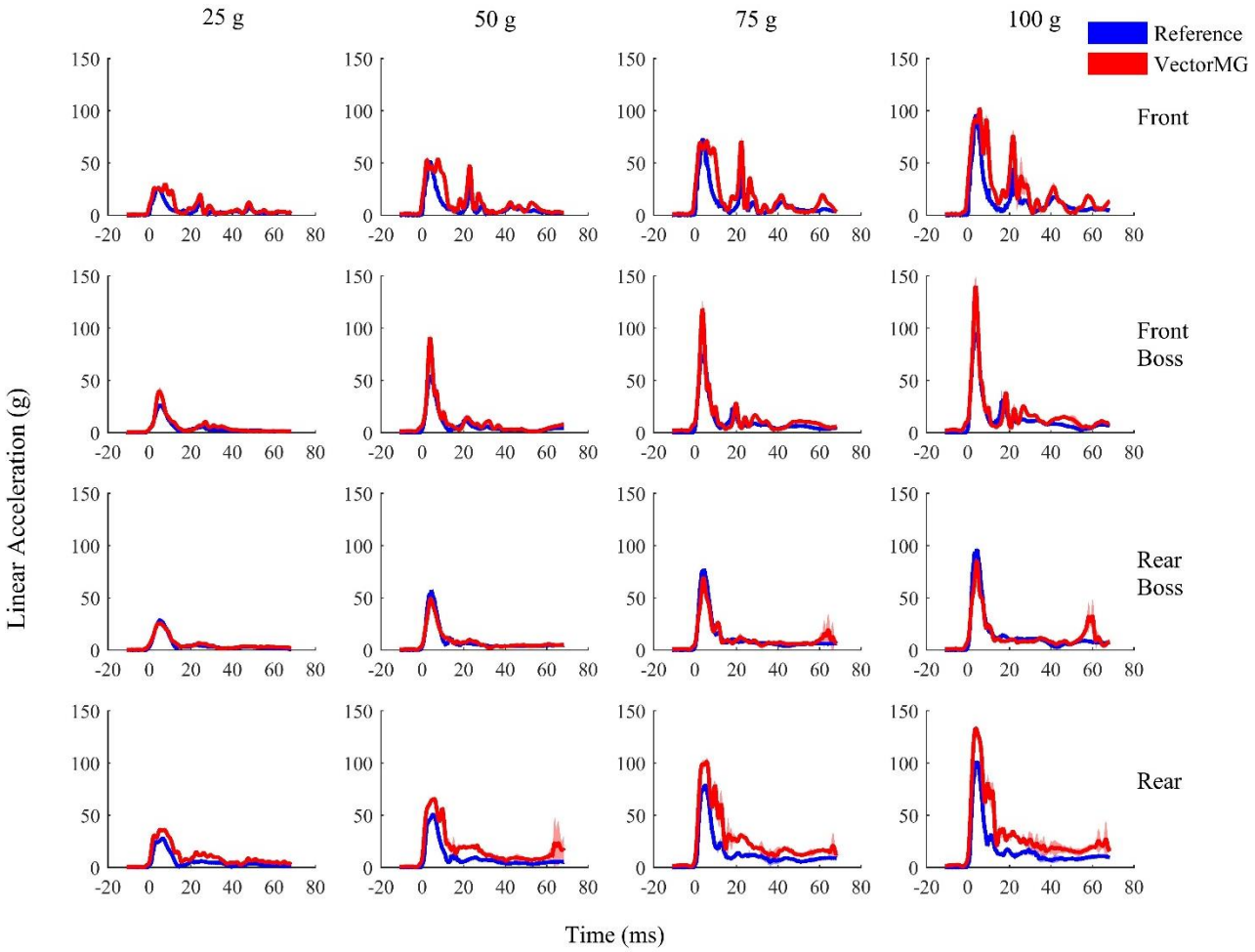

Figure A-5: Averaged helmeted Vector MG (red) and reference (blue) time series in linear acceleration. Vector MG front and rear locations had wider peaks than the reference. Front boss and rear locations also overpredicted reference peaks.

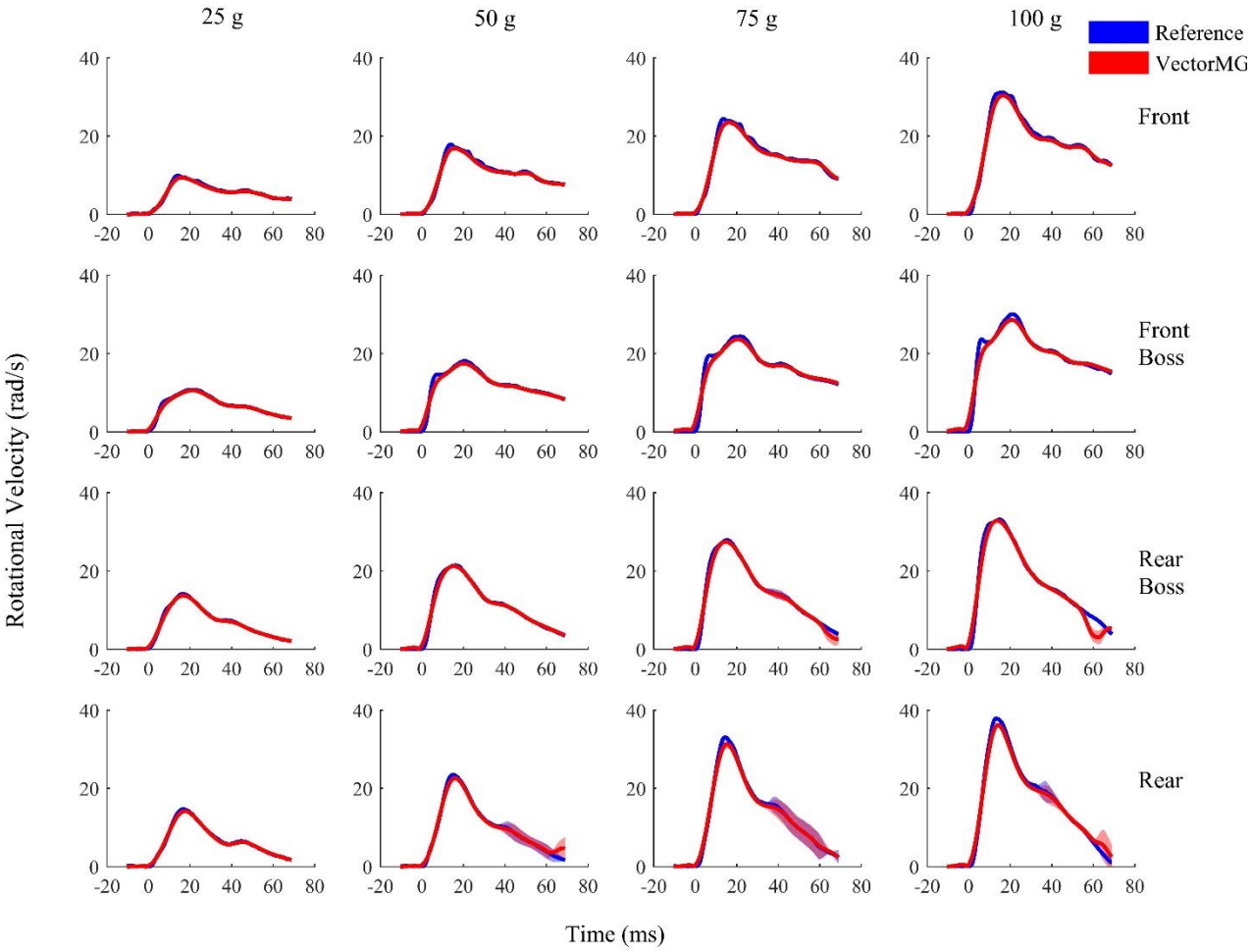

Figure A-6: Averaged helmeted Vector MG (red) and reference (blue) time series in rotational velocity. For all test conditions, Vector MG and reference curves exhibited many similarities in curve shape.

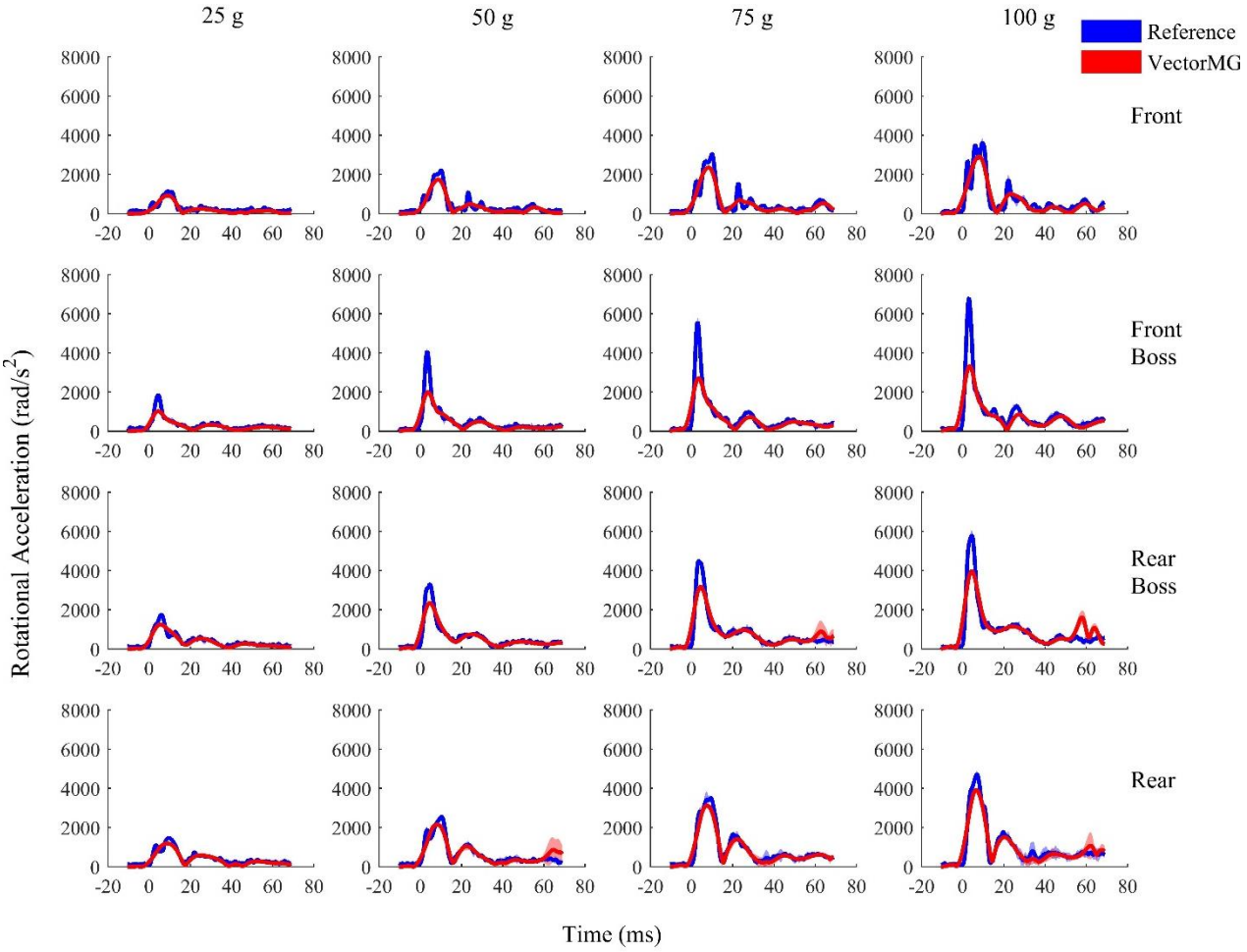

Figure A-7: Averaged helmeted Vector MG (red) and reference (blue) time series in rotational acceleration. Vector MG and reference curve shapes had overall similarities, although the sensor underpredicted the reference peaks in the front boss and rear boss locations.

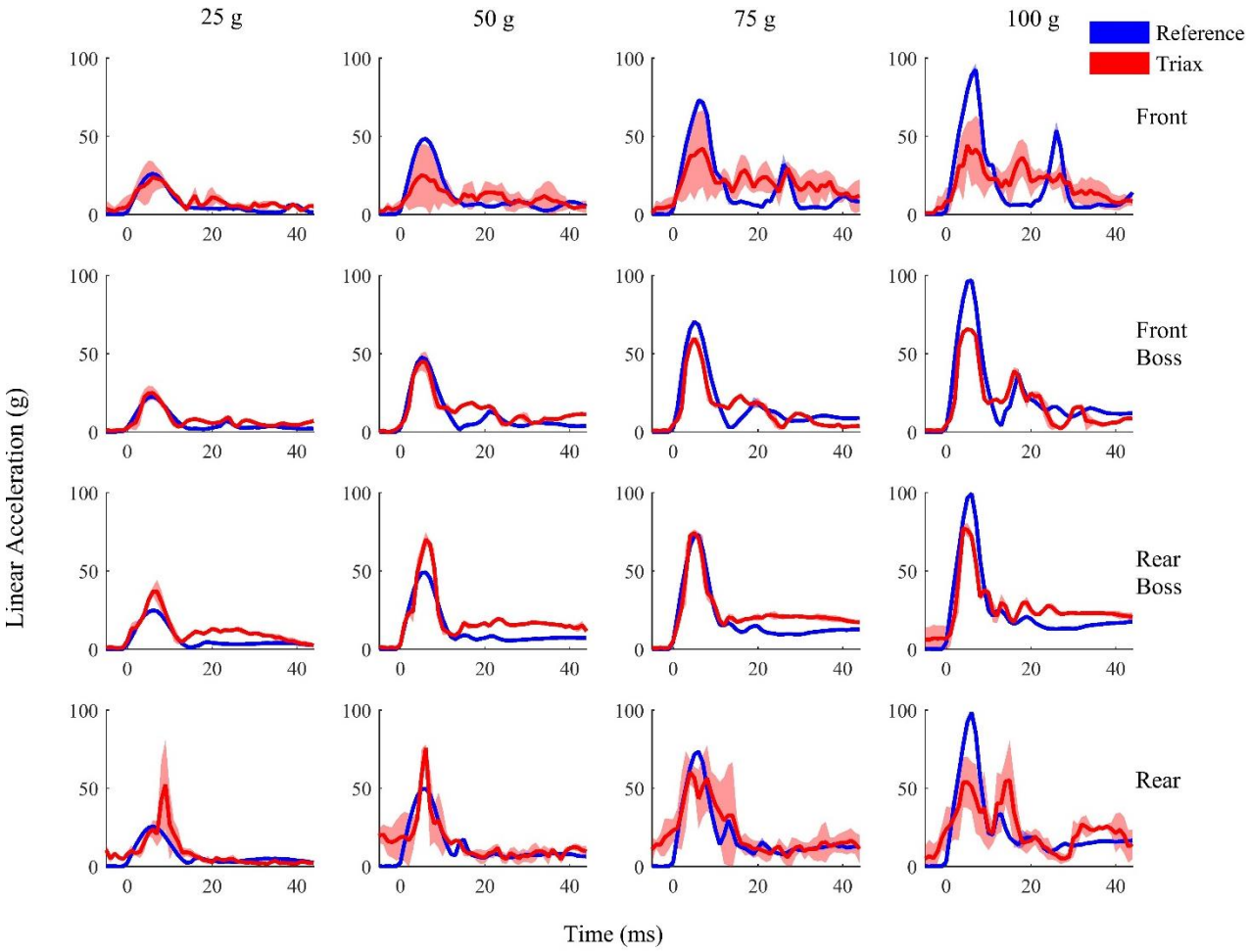

Figure A-8: Averaged unhelmeted Triax (red) and reference (blue) time series in linear acceleration. Triax exhibited a similar general peak shape to reference, although the sensors mostly underpredicted reference peaks. There were also large variations in the front and rear locations as illustrated by wide corridors.

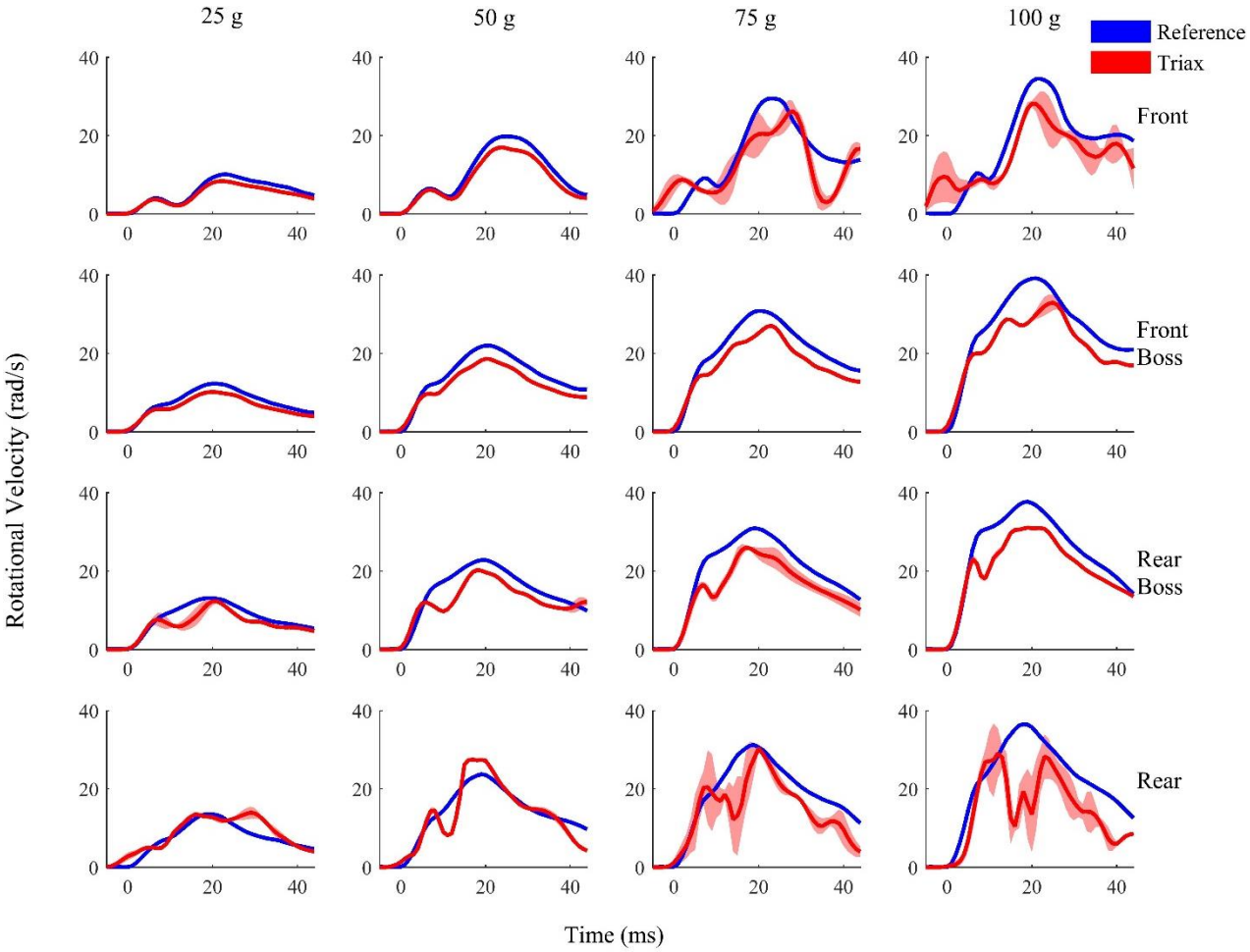

Figure A-9: Averaged unhelmeted Triax (red) and reference (blue) time series in rotational velocity. Triax exhibited a similar general peak shape to reference, although mostly underpredicted the peak. There were also large variations in the front and rear locations as illustrated by wide corridors.

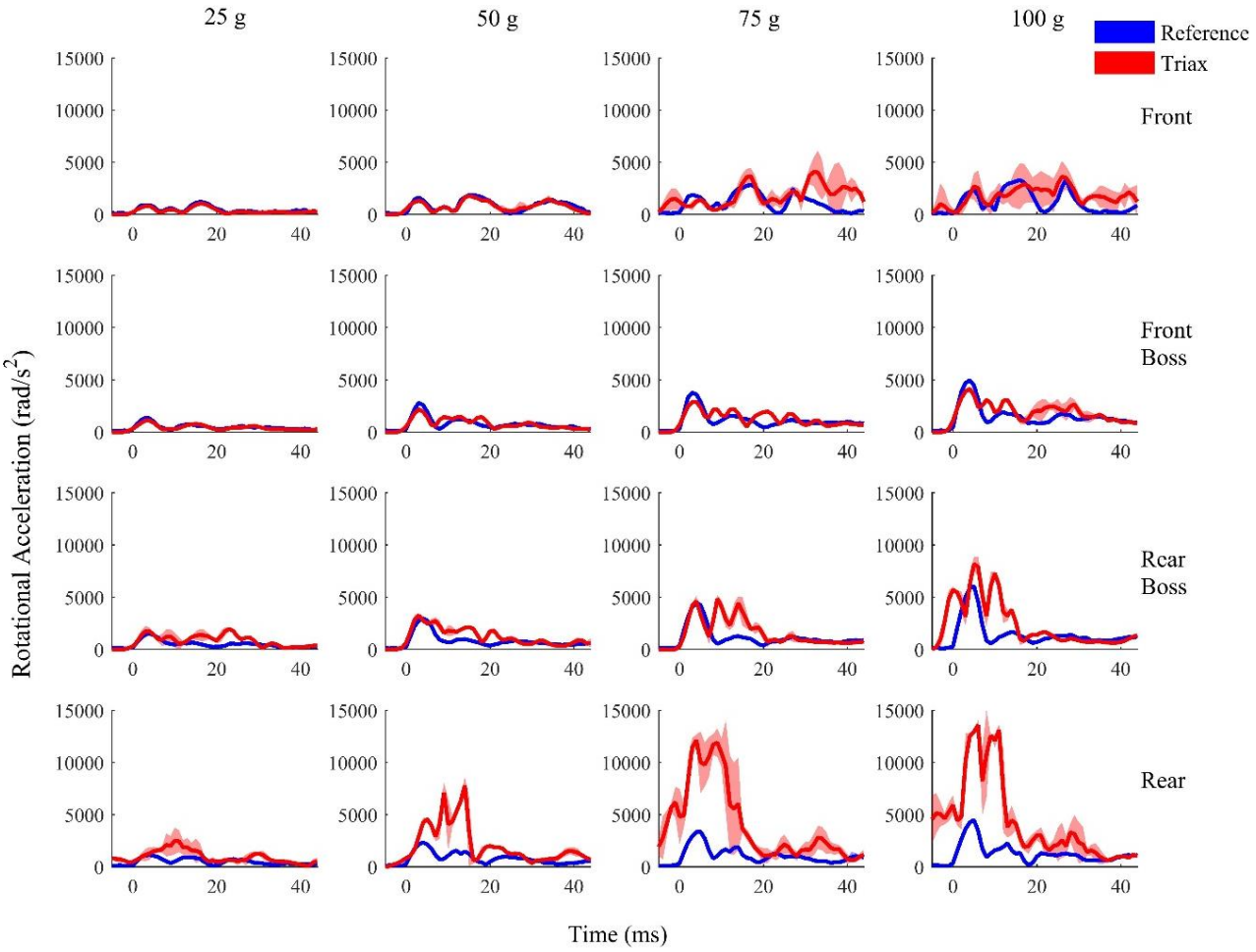

Figure A-10: Averaged unhelmeted Triax (red) and reference (blue) time series in rotational acceleration. Triax exhibited a similar curve shape in the low-energy front and front boss locations, but had multiple peaks and large variations for the other test conditions.

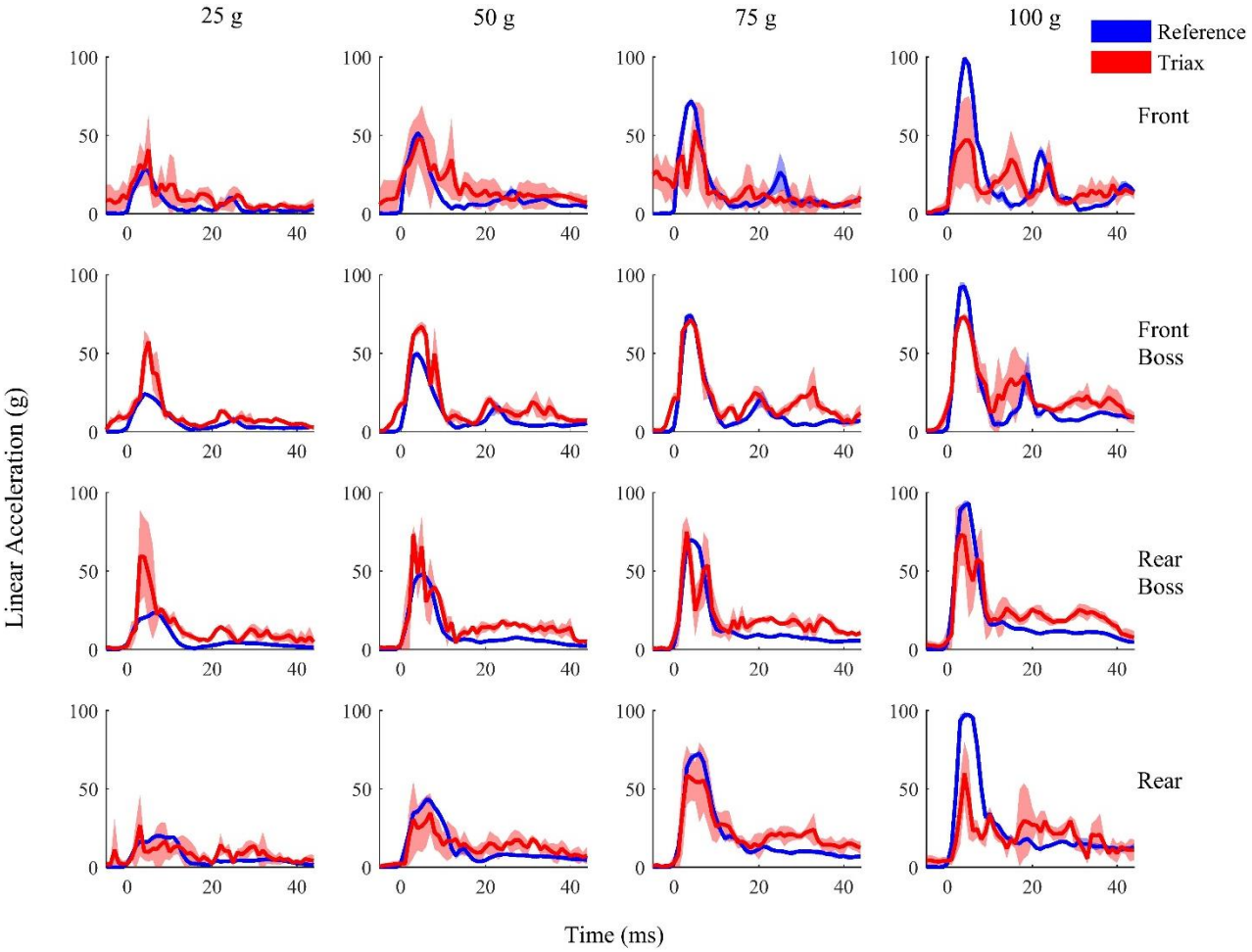

Figure A-11: Averaged helmeted Triax (red) and reference (blue) time series in linear acceleration. Triax exhibited a similar overall curve shape in the front boss location, but displayed large variability in the other locations as indicated by wide corridors.

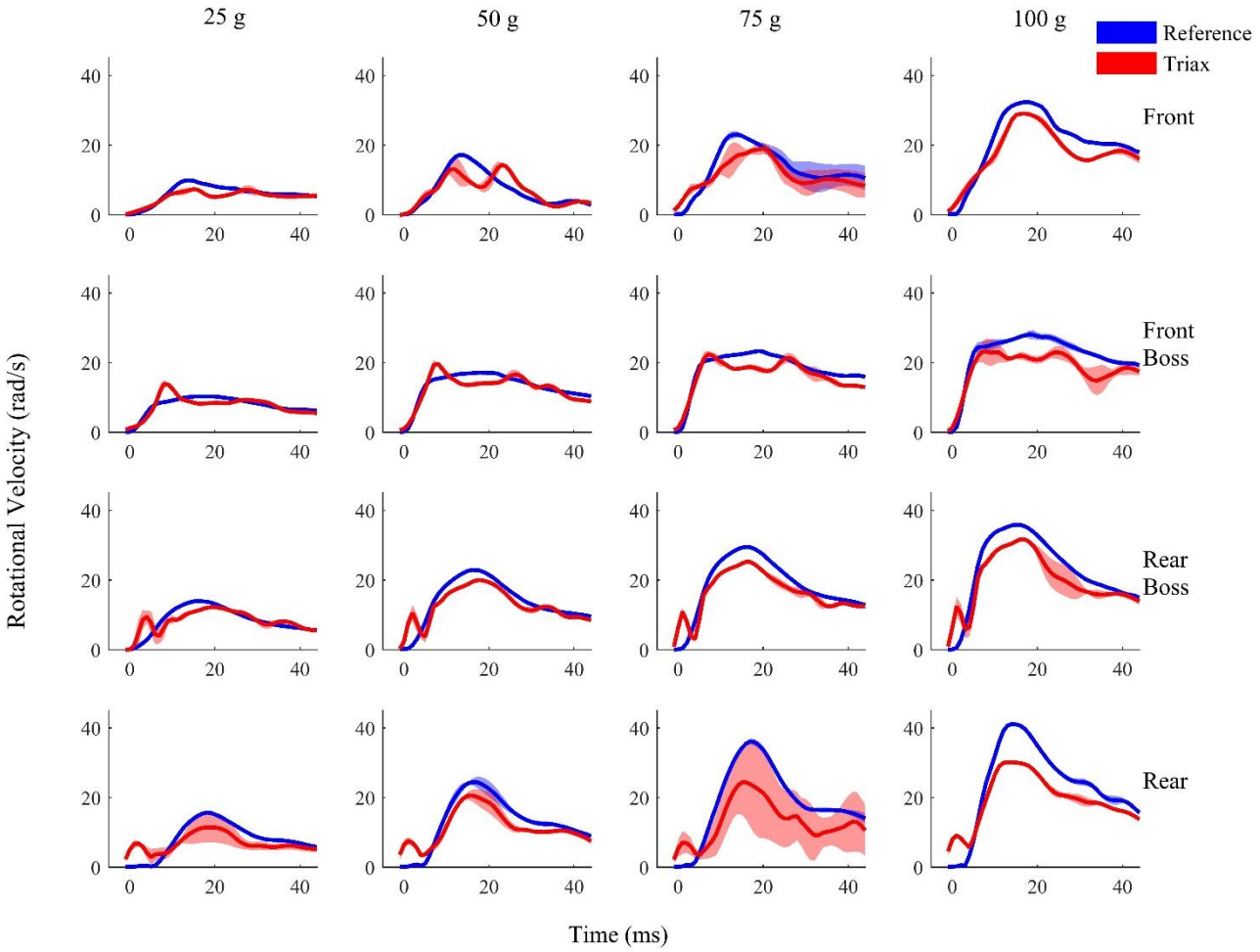

Figure A-12: Averaged helmeted Triax (red) and reference (blue) time series in rotational velocity. Triax exhibited a similar overall curve shape, but mostly underpredicted reference peaks.

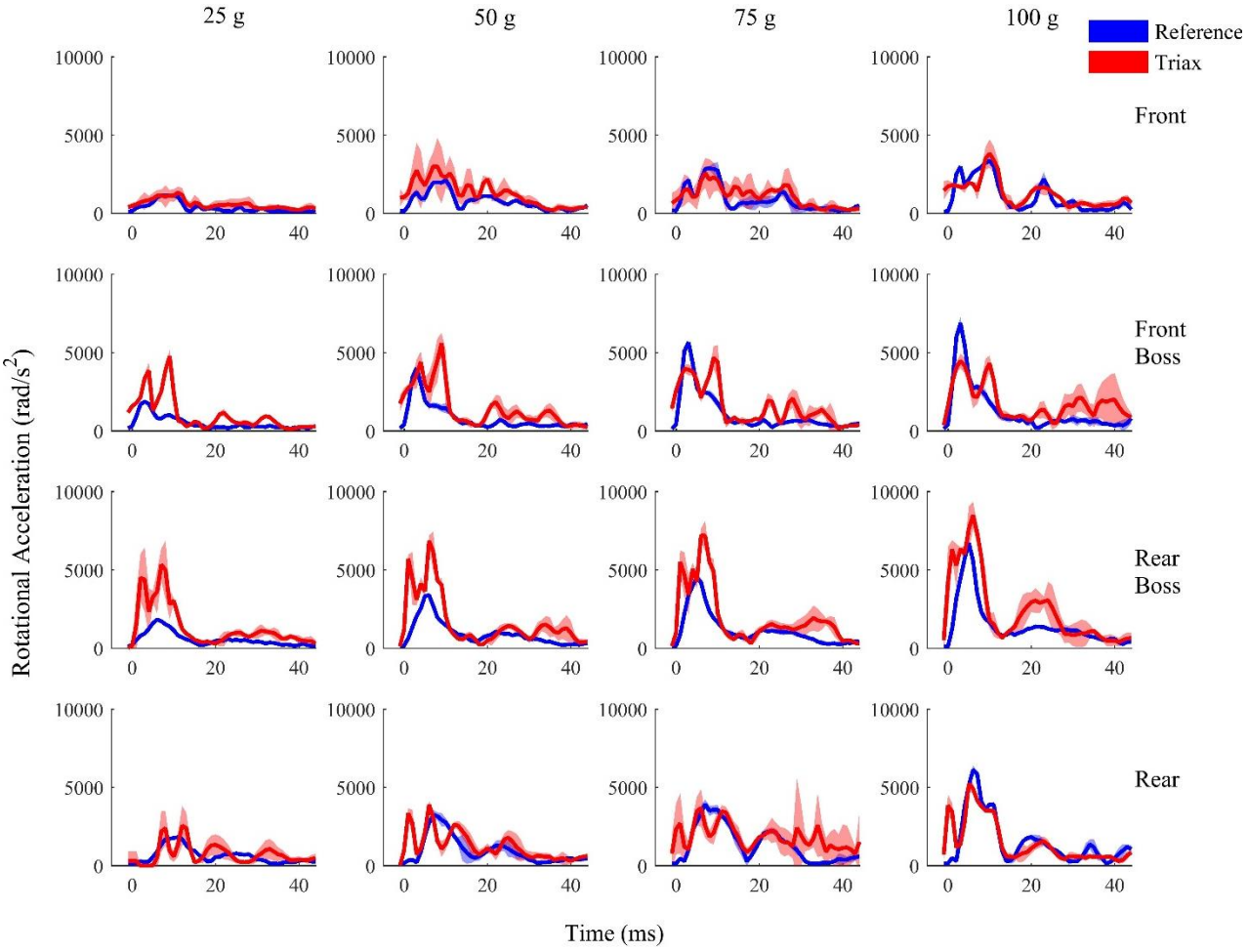

Figure A-13: Averaged helmeted Triax (red) and reference (blue) time series in rotational acceleration. Triax displayed dual peaks in many test conditions, making many curves dissimilar from the reference.

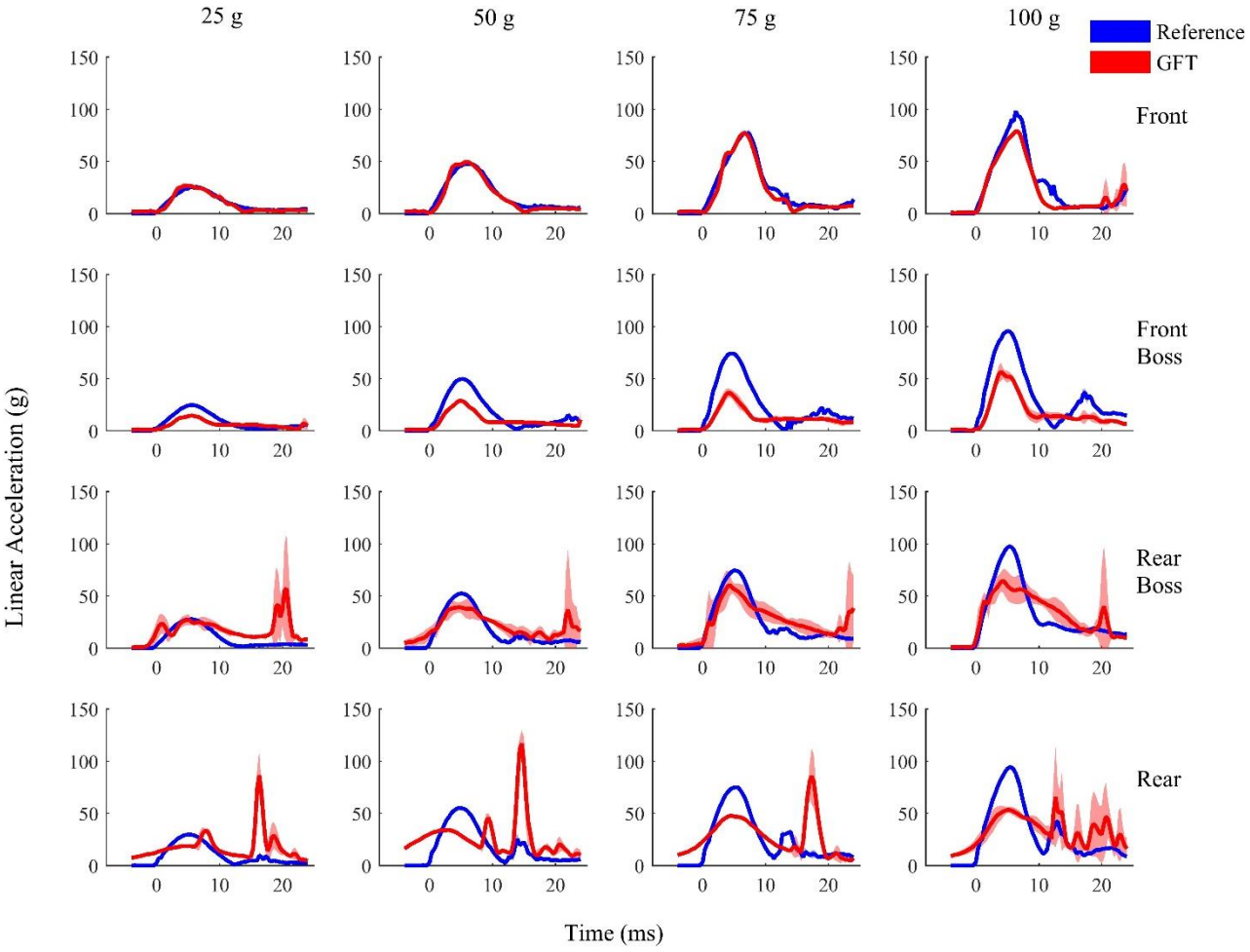

Figure A-14: Averaged unhelmeted GFT (red) and reference (blue) time series in linear acceleration. GFT displayed similarities to the reference for the front location, and underpredicted for the remaining locations. A second peak occurred in the rear boss and rear locations that may be caused by de-coupling of the headband from the headform, followed by a second impact.

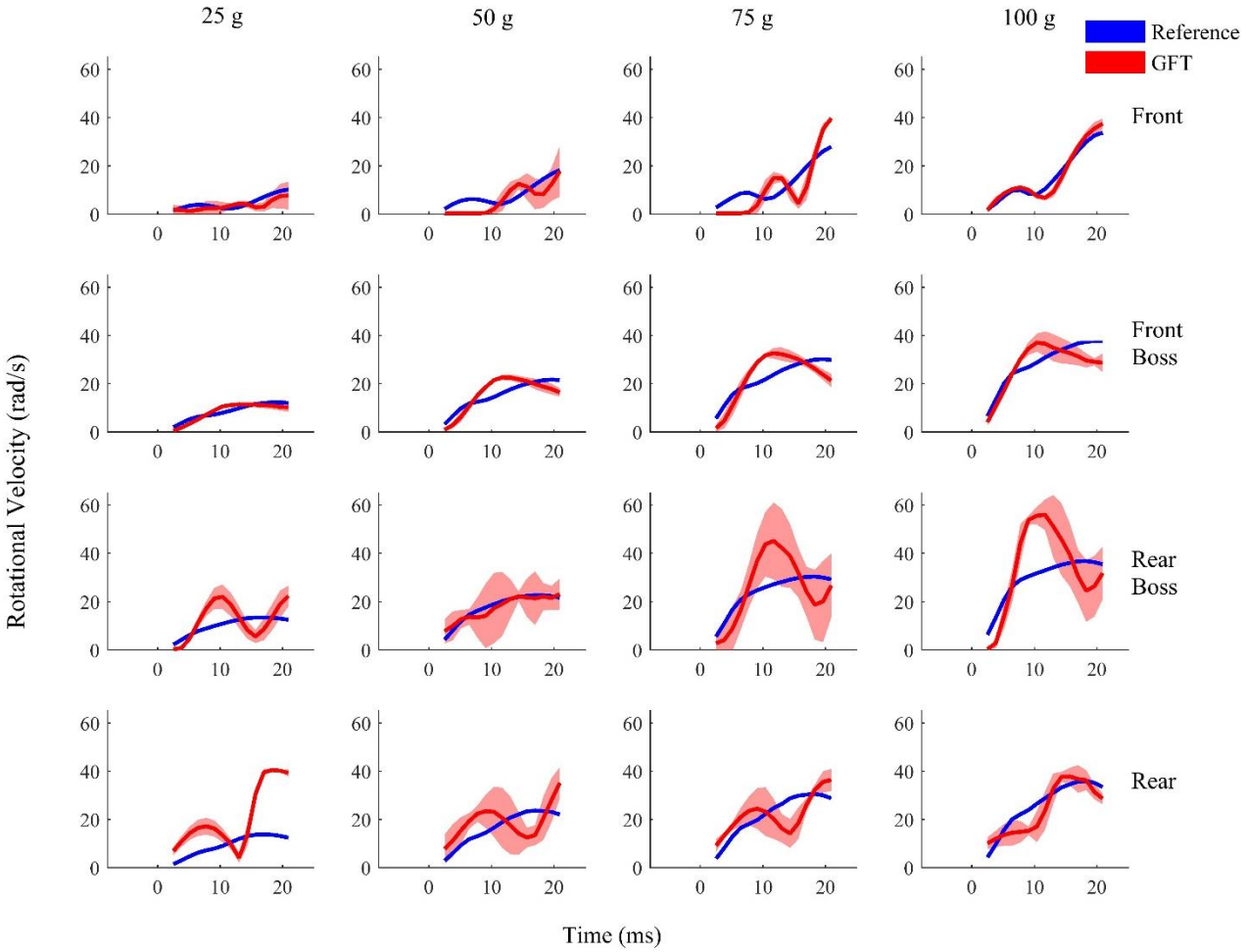

Figure A-15: Averaged unhelmeted GFT (red) and reference (blue) time series in rotational velocity. GFT curves were not very similar to reference and exhibited large variations in the rear boss and rear locations.

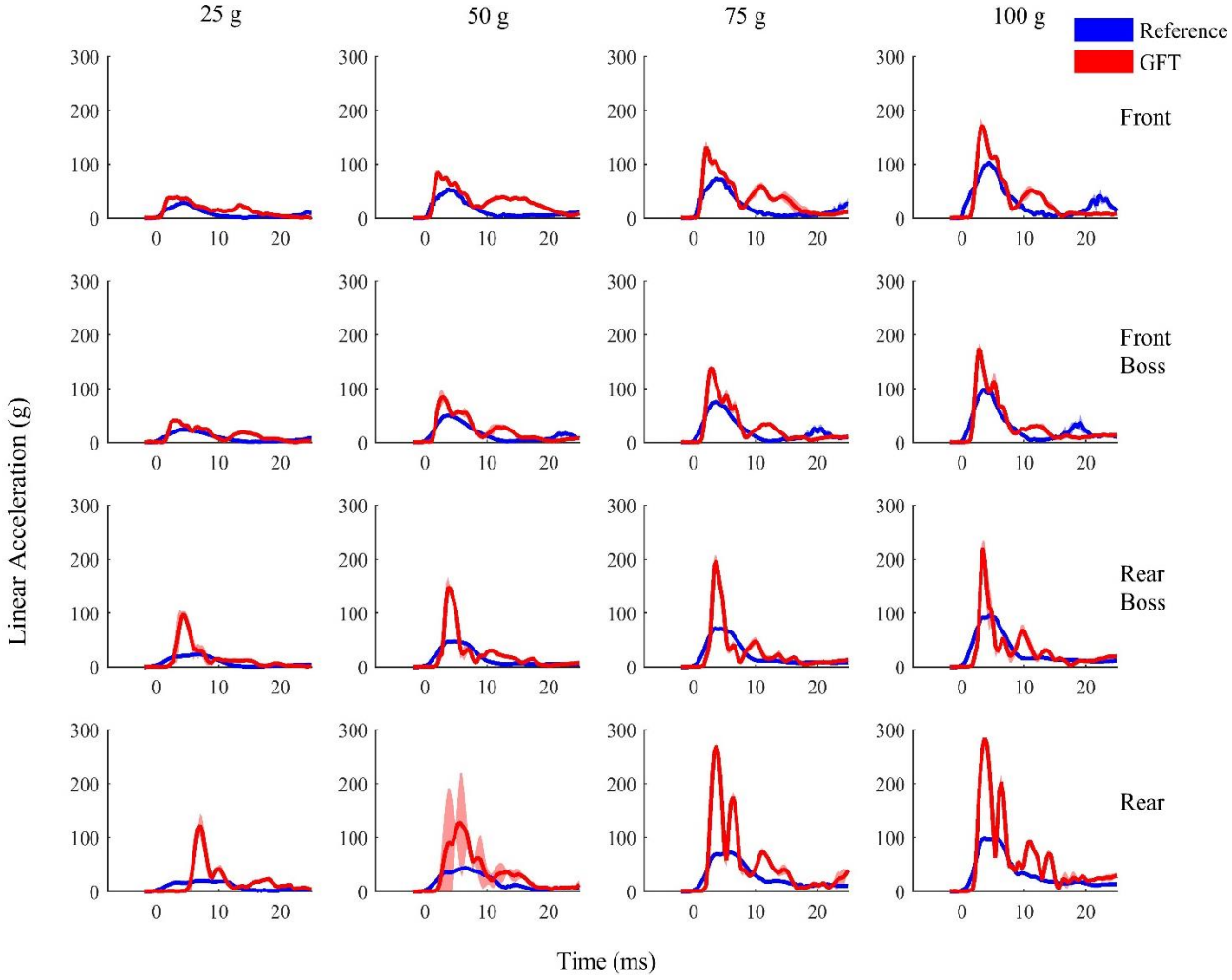

Figure A-16: Averaged helmeted GFT (red) and reference (blue) time series in linear acceleration. GFT largely overpredicted the reference, especially in the rear boss and rear locations. This may have been due to the proximity of the impact to the sensor placement on the helmet shell.

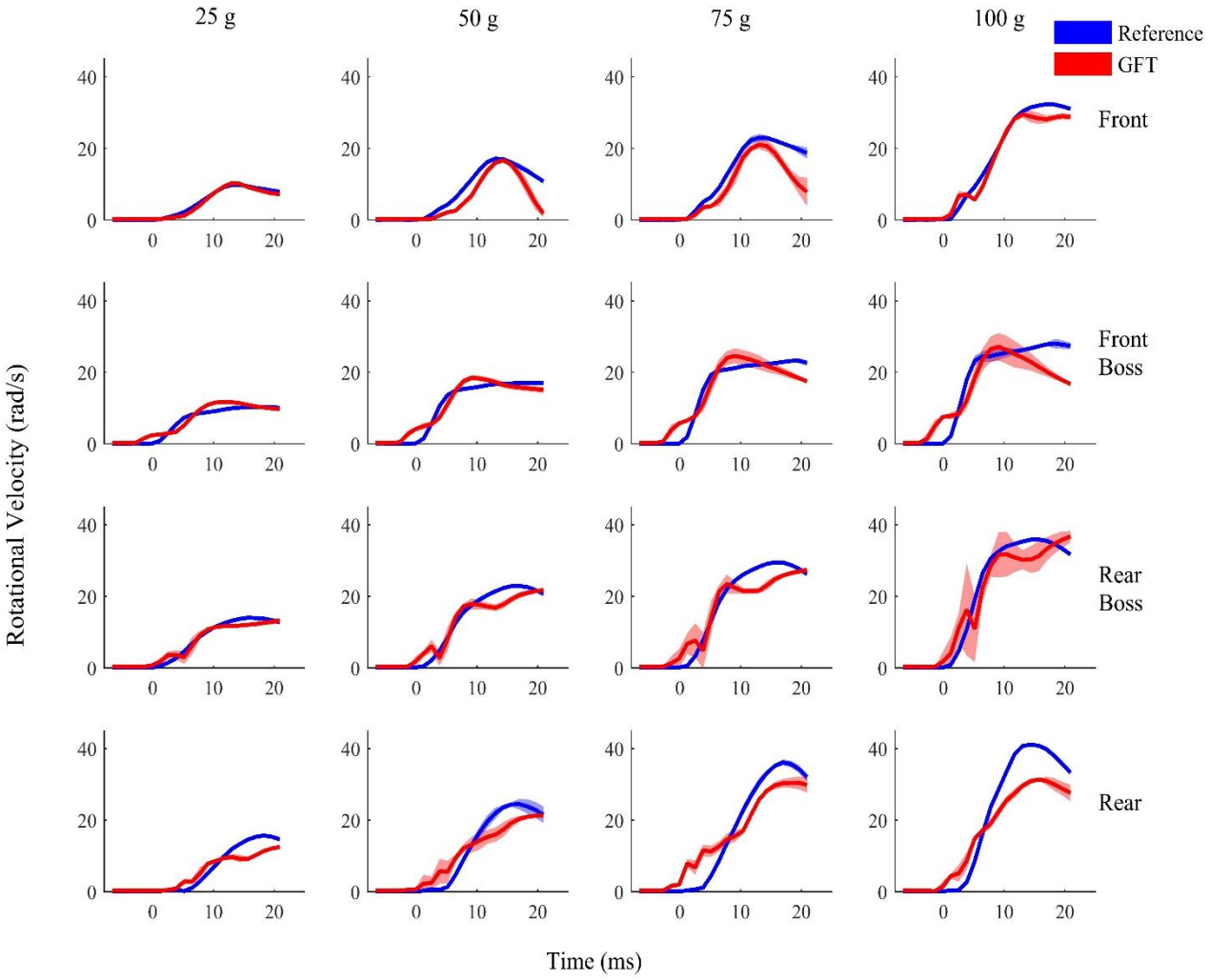

Figure A-17: Averaged helmeted GFT (red) and reference (blue) time series in rotational velocity. GFT aligns better with the references in rotational velocity than in linear acceleration, although the shapes are not entirely similar.